AD-A071 949 TEXAS A AND M UNIV COLLEGE STATION DEPT OF ELECTRICA--ETC F/G 20/12
ADMITTANCE BEHAVIOR IN GAAS SCHOTTKY IMPATT DIODES.(U)
1979 O EKNOYAN AFOSR-78-3567

UNCLASSIFIED AFOSR-TR-79-0872 NL

| OF |
AD
A071949

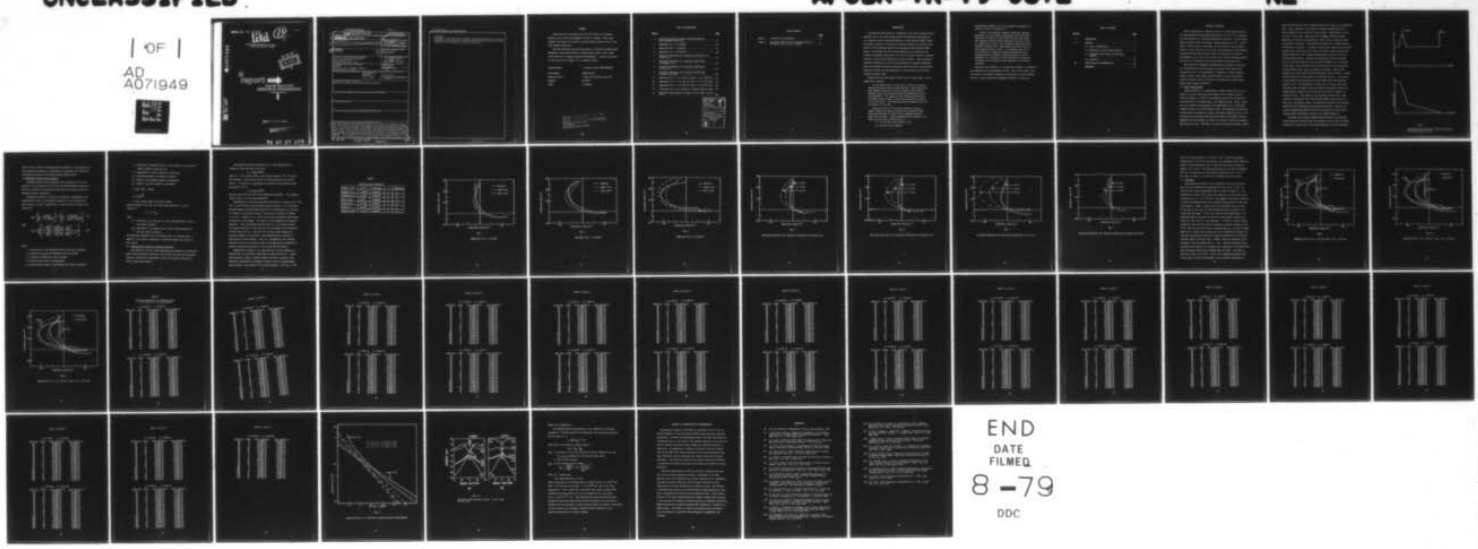

END
DATE
FILMED
8-79
DDC

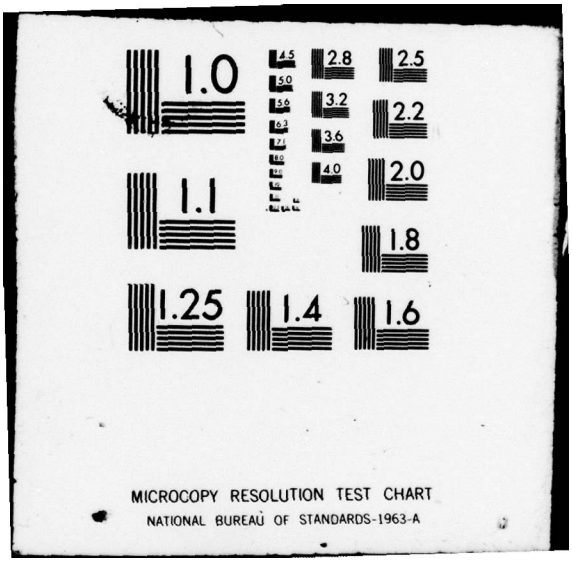
1.0
1.1
1.25
1.4
1.6
1.8
2.0
2.2
2.5
2.8
3.2
3.6
4.0
4.5
5.0
5.6
6.3
MICROCOPY RESOLUTION TEST CHART
NATIONAL BUREAU OF STANDARDS-1963-A

LEVEL

(13)

ADMITTANCE BEHAVIOR IN GaAs SCHOTTKY IMPATT DIODES

a report

from the Texas A&M
RESEARCH FOUNDATION
College Station, Texas

Unclassified

SECURITY CLASSIFICATION OF THIS PAGE (When Data Entered)

REPORT DOCUMENTATION PAGE

READ INSTRUCTIONS BEFORE COMPLETING FORM

1. REPORT NUMBER: AFOSR-TR-79-0872	2. GOVT ACCESSION NO.
3. RECIPIENT'S CATALOG NUMBER	
4. TITLE (and Subtitle): Admittance Behavior in GaAs Schottky IMPATT Diodes	5. TYPE OF REPORT & PERIOD COVERED: Final Report, 1 June 1978 — 31 May 1979
	6. PERFORMING ORG. REPORT NUMBER
7. AUTHOR(s): O. Eknoyan	8. CONTRACT OR GRANT NUMBER(s): AFOSR-78-3567
9. PERFORMING ORGANIZATION NAME AND ADDRESS: Electrical Engineering Department, Texas A&M University, College Station, TX 77840	10. PROGRAM ELEMENT, PROJECT, TASK AREA & WORK UNIT NUMBERS: 61102F, 2305D9
11. CONTROLLING OFFICE NAME AND ADDRESS: AFOSR/NE, Electronic and Solid State Sciences, Bolling AFB, D.C. 20332	12. REPORT DATE: 1979
	13. NUMBER OF PAGES: 46
14. MONITORING AGENCY NAME & ADDRESS (if different from Controlling Office): 49 p.	15. SECURITY CLASS. (of this report): Unclassified
	15a. DECLASSIFICATION/DOWNGRADING SCHEDULE

16. DISTRIBUTION STATEMENT (of this Report)
Approved for public release; distribution unlimited

17. DISTRIBUTION STATEMENT (of the abstract entered in Block 20, if different from Report)

18. SUPPLEMENTARY NOTES

19. KEY WORDS (Continue on reverse side if necessary and identify by block number)

20. ABSTRACT (Continue on reverse side if necessary and identify by block number)

This report presents the results of efforts, all of which are related to ionization rate effects on the admittance behavior of Low-High-Low gallium-arsenide (LHL GaAs) Schottky IMPATT diodes. The analysis were made using an improved equivalent circuit model which was developed earlier. The effects of reported different ionization rates in GaAs as well as newly generated ones were calculated and compared with experimentally measured admittance data. Generally, good agreement has been obtained. It is observed that (i) at low currents, the resonant frequency is less that the cutoff frequency and (ii) at high currents, the admittance behavior is

DD FORM 1 JAN 73 1473

410 214

UNCLASSIFIED

20 (cont.)
capacitive. The results also indicate the possible existence of injection mechanisms other than impact ionization which become most apparent at high fields and are influenced by crystal orientation.

FORWARD

This project was initiated by the Air Force Office of Scientific Research and is under the management of Major C. Gardner. This report presents the results of the entire research program conducted from 1 June 1978 through 31 May 1979.

The work described herein was performed at the Electrical Engineering Department, Texas A&M University, College Station, Texas 77843, under the direction of O. Eknoyan (principal investigator). Another contributor to this work was H.K. Lesser, Jr., a graduate student.

Program Manager	C. Gardner, Major USAF(AFOSR/NE)
Grant Number	AFOSR-78-3567
Reporting Period	1 June 1978 through 31 May 1979
Prepared	May 1979
Author	O. Eknoyan

LIST OF ILLUSTRATIONS

LIST OF TABLES

INTRODUCTION

The work described herein is a summation of the entire research effort conducted from 1 June 1978 through 31 May 1979 regarding investigations in a program entitled "Admittance Behavior in GaAs Schottky IMPATT Diodes". The primary objective of this work has been to examine the ionization rate effects on the admittance behavior of low-high-low GaAs Schottky IMPATT diodes, and determine the most optimum ionization rate expression and suitable coefficients which need to be used in conjuction with an improved equivalent circuit model developed for such structures. Other objectives included investigation on the possible existence of injection mechanisms other than avalanche multiplication which could contribute to such devices admittance behavior and the examination of factors which may influence avalanche response times.

Progress has been successfully made in each of these areas, and are summarized as follows:

In the initial phase of this study, a survey on existing reported ionization rates for GaAs was made. Those expressions were assesed in conjunction with an improved device model to determine which will best agree with the experimentally measured admittance. The results of that effort were described in an earlier progress report and are also summarized in Section 2.3 of this report. The expression given by Logan and Sze [11] was found to be the best.

Using the results of the initial phase as a basis, a digital computer was used to generate new ionization coefficients and determine if better fits of admittance measurements could be found. Several expressions were examined. Of these, the two best for electrons are

$$\alpha = 4.5 \times 10^5 \exp\left[-(8 \times 10^5/E)^2\right] \text{ and}$$

$$7.5 \times 10^5 \exp\left[-(9 \times 10^5/E)^2\right].$$

The admittance behavior for all the examined expressions are listed in table II of Section 2.3.

Finally, the different ionization rates were analyzed. Indications are that injection mechanisms other than impact ionization are likely in such devices and that they become most apparent under high field conditions and certain crystal orientations, which in turn influences injections during avalanche response times. These mainly stem from the electronic band structure in GaAs. It is believed that due to the conditions of energy and momentum conservation interconduction band or tunneling could exist which may be responsible for a time delay in the acceleration of electrons (or holes) to the threshold energy required for initiating ionization.

Generally good agreement for the admittance behavior is obtained in the comparisons with experimental results. They indicate that (i) at low currents the resonant frequency is less than the cutoff frequency and (ii) at high currents the admittance behavior is capacitive.

TABLE OF CONTENTS

SECTION II ANALYSIS

Severe limitations in elemental silicon, Si, semiconductor material for high frequency and high speed applications, has led to the consideration and growing use of compound semiconductor materials. In this regard, gallium-arsenide, GaAs, has become a strong competitor with Si. This is simply a direct result of the higher low field mobility and saturation velocity in GaAs relative to Si [1] [2], the availability of semi-insulating GaAs substrate material which permits the reduction of parasitic capacitances [3] [4], plus the fact that it is a direct band-gap material and as such its ionization rates differ markedly from those of Si.

With this well recognized and demonstrated advantages of GaAs over Si, considerable work has been going on to develop GaAs devices and integrated circuit, IC, technologies, in addition to several numerous studies focused on some basic questions which are often raised about physical processes that are involved in the operation of GaAs devices which requires impact ionization.

2.1 Basic Considerations

Impact ionization in a semiconductor junction diode occurs when an electron (or hole) gains sufficient energy, from an applied electric field for example, to create an electron-hole pair by the ionization of an electron from the valence band to the conduction band. Impact ionization can therefore be considered as the amplification of an externally injected current in a strong electric field. The avalanche gain produced by this manner is measured in terms of the impact ionization rates, α for electrons and β for holes, which gives the number of secondary carriers generated per unit distance of travel in an electric field by an initiating electron or hole. Generally, the rates are not equal and many studies

have long been made [5]-[8] to establish theoretical basis for understanding them. Impact ionization, also known as avalanche multiplication, is a basic mechanism in the operation of many devices. IMPATT diodes are only one type in this class. They operate in the IMPact Avalanche Transit Time mode, and they are charcterized for their ability to generate power at microwave frequencies. Under operating conditions, an IMPATT diode is divided into two regions. An avalanche (high field) region where avalanche multiplication takes place, and a drift (low field) region through which carriers produced by the avalanche multiplication travel at their scattering limited velocity. Studies have indicated that [9] the maximum dc to rf conversion efficiency and rf power of IMPATTs can be increased if the ratio of the voltage drop in the drift zone to the voltage drop in the avalanche zone, V_D/V_A, is allowed to increase. Devices with favorable such ratios have long been fabricated from Si material. Indeed, the Read structure [1] has proved to be the most suitable. The interest in GaAs IMPATTs resulted mainly from their lower noise charcteristics relative to Si. The realization of large ratio for V_D/V_A, hence high efficiency Read like GaAs devices was achieved by properly varying the doping density (profile) near the junction side which is formed by a Schottky contact. This evolved in the discovery of high power, high efficiency Low-High-Low (LHL) GaAs Schottky IMPATT diodes, Figure [1]. Since then, considerable effort, and significant advances have been made concerning their fabrication and microwave performance. However, admittance measurements obtained from such LHL devices [10] have shown a behavior which is different than that of Si IMPATT diodes [1].

In recent years, several experimentally determined and different results have been reported about the ionization rates in GaAs [11]-[18]. As opposed to silicon [19], it has been difficult to use the published

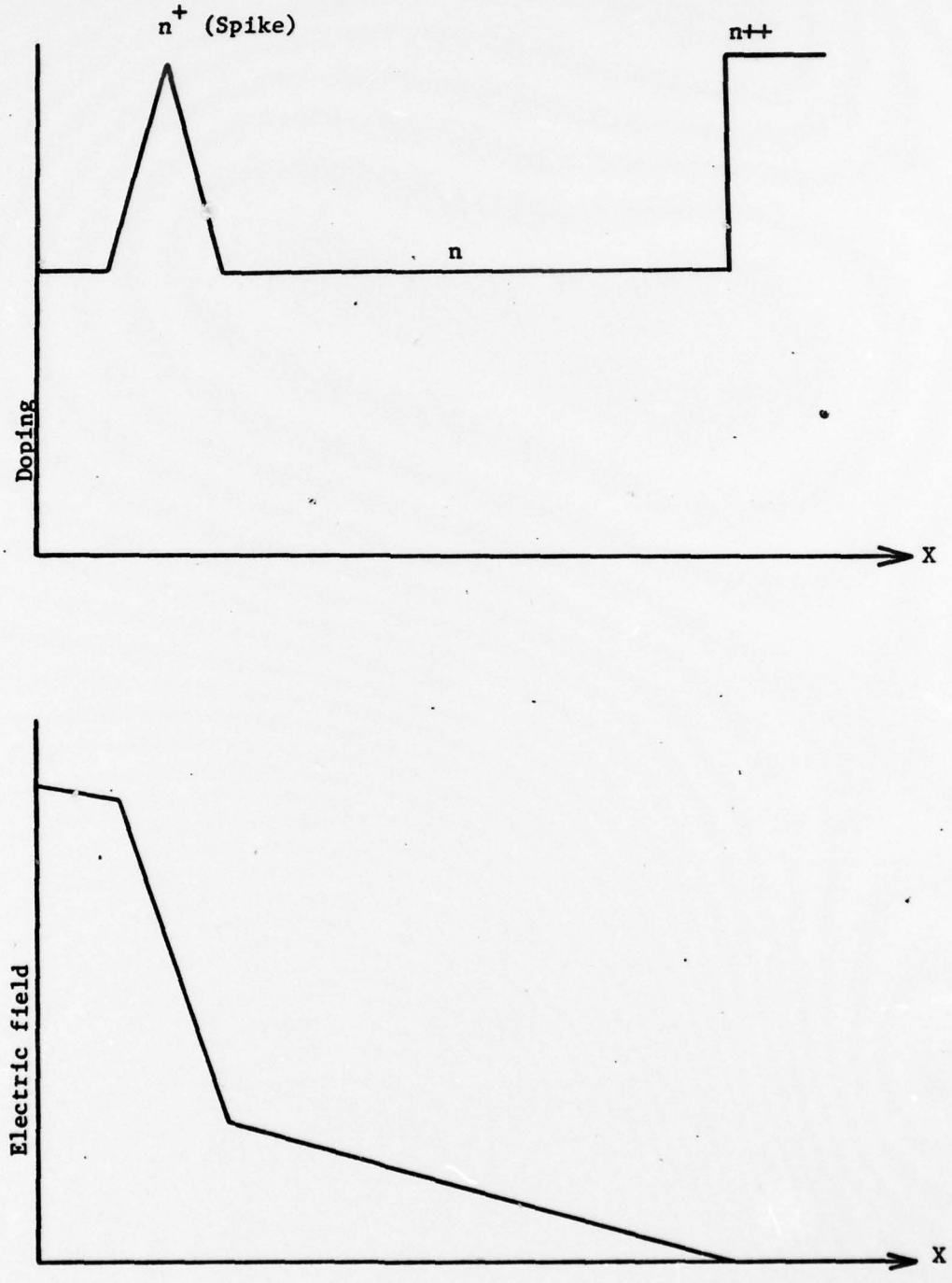

Fig. 1

Idealized Doping and Electric Field Distributions
for Low-High-Low Structures

rates of GaAs to model an avalanche diode successfully. The inception of this program was primarily to investigate the ionization rate effects on the admittance behavior of LHL GaAs Schottky IMPATT diodes.

2.2 Highlights of Small Signal Analysis

Following Gilden and Hines approach [20], expressions for the admittance of the avalanche zone and drift zone were determined separately. The total impedance of the diode was then taken as the sum of these two individual region's impedances.

Including the effects of dielectric relaxation, recombination, and multiplication factor, the normalized admittance of the avalanche and drift regions, Y_a and Y_d respectively in, mhos per square centimeter are obtained as:

$$Y_a = \left[\frac{\sigma}{X_a} + \frac{2\alpha' J_o B}{B^2 + (\omega\tau_a)^2}\right] + j\left[\frac{\omega\varepsilon}{X_a} - \frac{2\alpha' J_o(\omega\tau_a)^2}{\omega\tau_a(B^2 + \{\omega\tau_a\}^2)}\right] \quad (1)$$

and

$$Y_d = j\frac{\omega\varepsilon}{X_d}\left[\frac{1 - \left(\frac{\omega}{\omega_a}\right)^2 + j\left(\frac{\omega}{\omega_a}\right)^2\left(\frac{1}{\omega t_r} + \frac{2}{\omega M\tau_a}\right)}{1 - \left(\frac{\omega}{\omega_a}\right)^2 + j\left(\frac{\omega}{\omega_a}\right)^2\left(\frac{1}{\omega t_r} + \frac{2}{\omega M\tau_a}\right) + j\beta}\right] \quad (2)$$

where:

σ = conductivity in the avalanche region in mhos per centimeter.

τ_a = transit time across the avalanche retion in seconds.

t_r = effective recombination time in seconds.

M = multiplication factor, dimensionless.

J_o = diodes current density in milliampers per square centimeters

α' = derivative of ionization rate, α, with respect to the electric field in number of ions per volt.

ϵ = permittivity of GaAs in farads per centimenter

ω_a = avalanche frequency in radians per second.

X_a = length of the avalanche region in centimeters.

X_d = length of the drift region in centimeters.

$B = \frac{\tau_a}{t_r} + \frac{2}{M}$, a constant

$\beta = \frac{1 - e^{-j\theta}}{\theta}$

$\theta = \omega\tau_d$, transit angle in the drift region.

Using equations (1) and (2), the total diode admittance, Y, can be written as:

$$Y = Y_r + jY_{im}$$

where:

Y_r = conductance, the real part of total diode admittance in mhos per square centimeter.

Y_{im} = susceptance, the imaginary part of total diode admittance in mhos per square centimeter.

The admittance expression for the avalanche zone, Y_a, indicates that in addition to the reactive components, a resistive element also exists in this region.

2.3 Ionization Rate Effects on Admittance Behavior

The behavior of the total diode admittance was examined by calculations using reported different ionization rates of GaAs plus some newly generated ones and, comparing with experimental results for devices fabricated on <100> oriented GaAs material.

The reported different expressions for α, were compiled from a literature survey and were of the form:

$$\alpha = a \exp[-(b/E)^m]$$

where "E" is the critical field in the avalanche region, "a", "b" and "m" are constants. The different values of these parameters are listed in Table 1. In addition, an expression for ionization rates given by Okuto and Crowell [17] as:

$$\alpha = aE \exp[-(b/E)^m]$$

was also used, where "a" and "b" are temperature dependent. The constants shown in Table I are for room temperature.

Computations of total diode admittance were made for values of "M" = 500, "E" = 5×10^5 volts/cm, and scattering limited velocity V = 9×10^6 cm/sec. The experimental and theoretical behaviors of the admittance as a function of frequency for different values of bias currents are shown in Figures 2, 3, and 4. Figures 5, 6, 7, and 8 are for other ionization coefficients as indicated on the figures. The results of the comparison are generally supportive. They consistently indicate that (i) at low current density the resonant frequency is less than the cutoff frequency (for definitions of these terms see [1], p. 222) and (ii) at high current density the admittance behavior is capacitive. Both observations are contrary to conventional Si diode behavior. This is a consequence of the different ionization rates of Si and GaAs as well as the high fields encountered in narrower avalanche regions such as that of the LHL GaAs devices.

Examination of Figures 2 - 8, indicates that the best agreement is obtained with the ionization coefficients of Logan and Sze [11]. Using these values as a basis, a digital computer was used to generate other ionization coefficients to determine if better fits of the measurements could be found. The constant "a" was varied between 2×10^5 and 9×10^5,

Table I

Ionization Rate Parameters

Authors' Name	$a(cm^{-1})$	b(volt/cm)	m	Reference
Salmer et al	1.18×10^5	5.55×10^5	2	14
Wisseman et al	1.6×10^5	5.55×10^5	2	15
Hall & Leck	2×10^5	5.55×10^5	2	12
Logan & Sze	3.5×10^5	6.85×10^5	2	11
Ito et al	5.6×10^6	2.41×10^6	1	17
Okuto & Crowell	$2.94.10^{-1}$	5.86×10^5	2	18

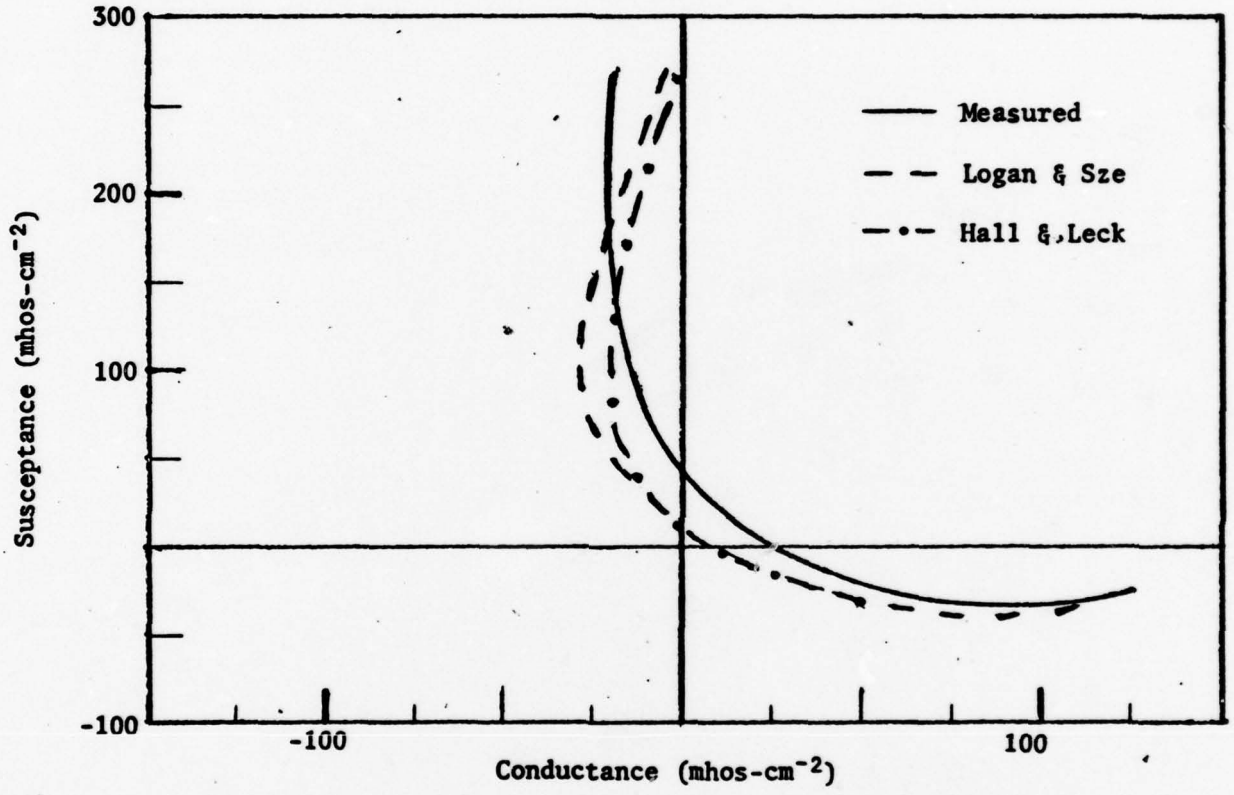

Fig. 2

Admittance for J = 25 mA/cm^2

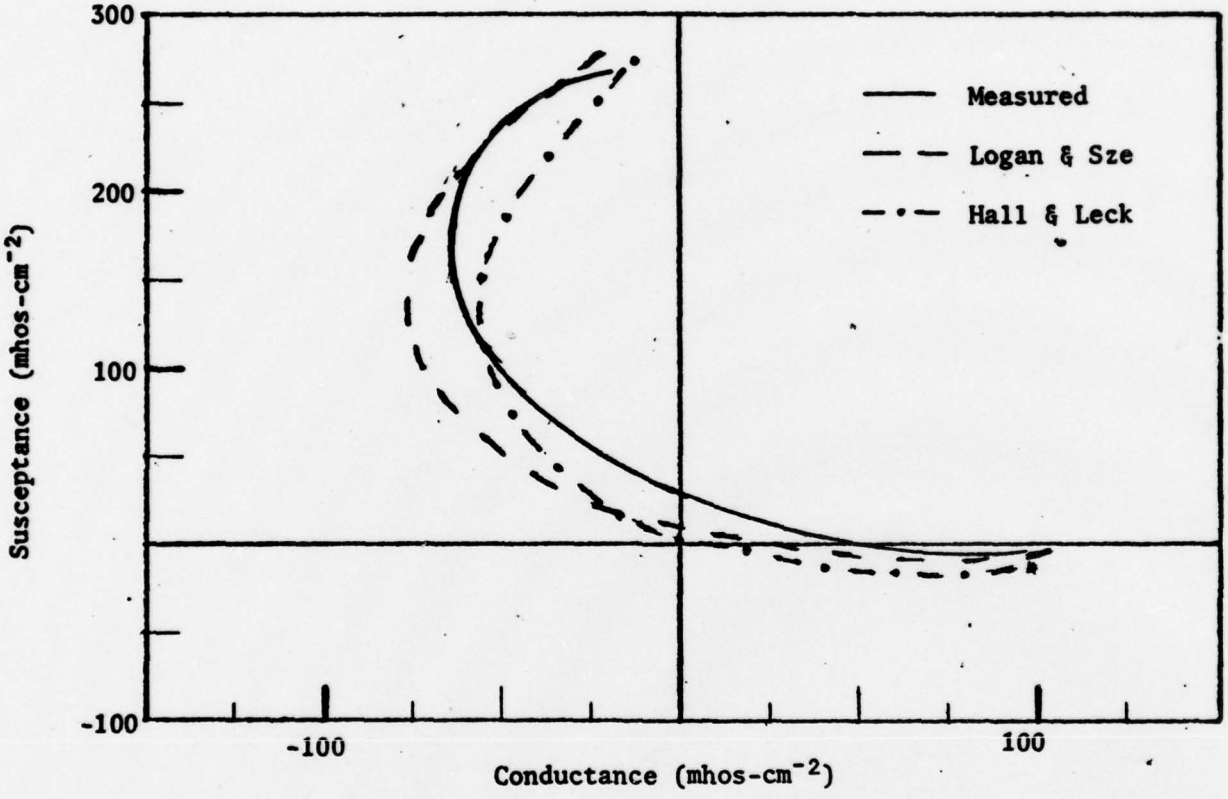

Fig. 3

Admittance for J = 75 mA/cm^2

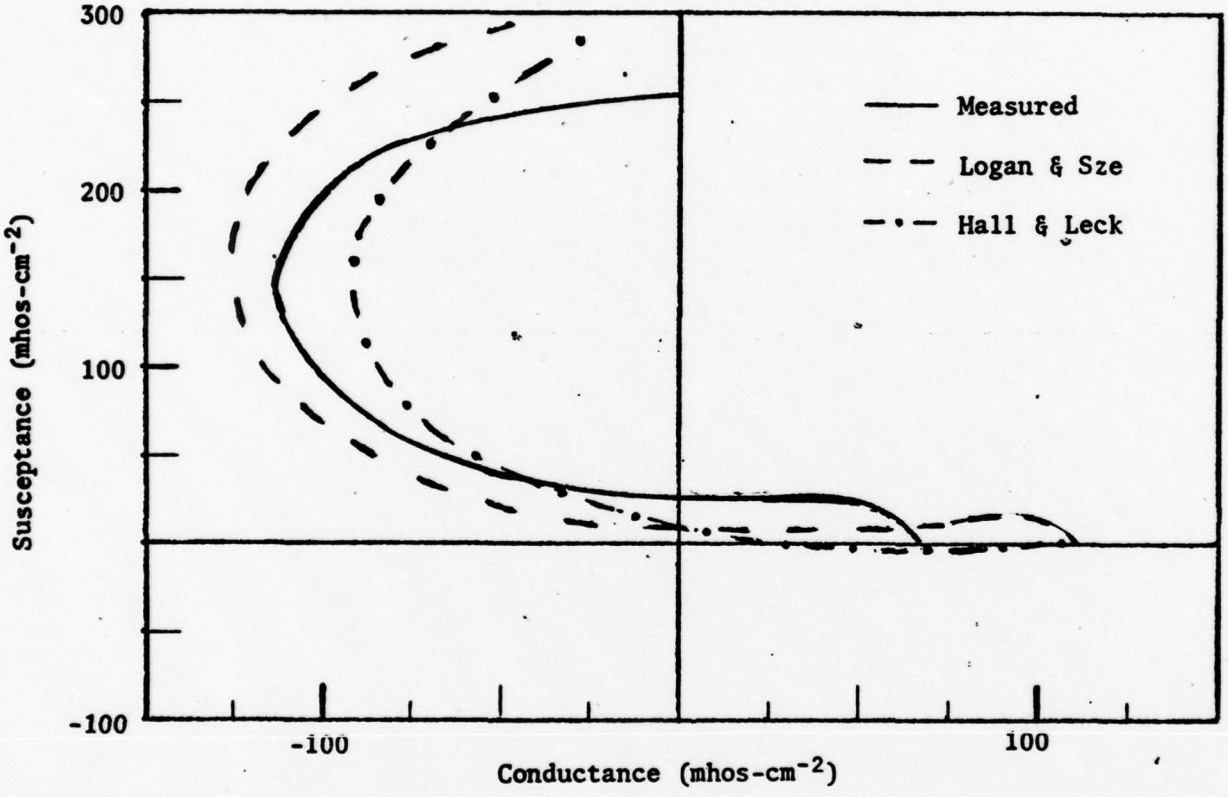

Fig. 4

Admittance for J = 125 mA/cm^2

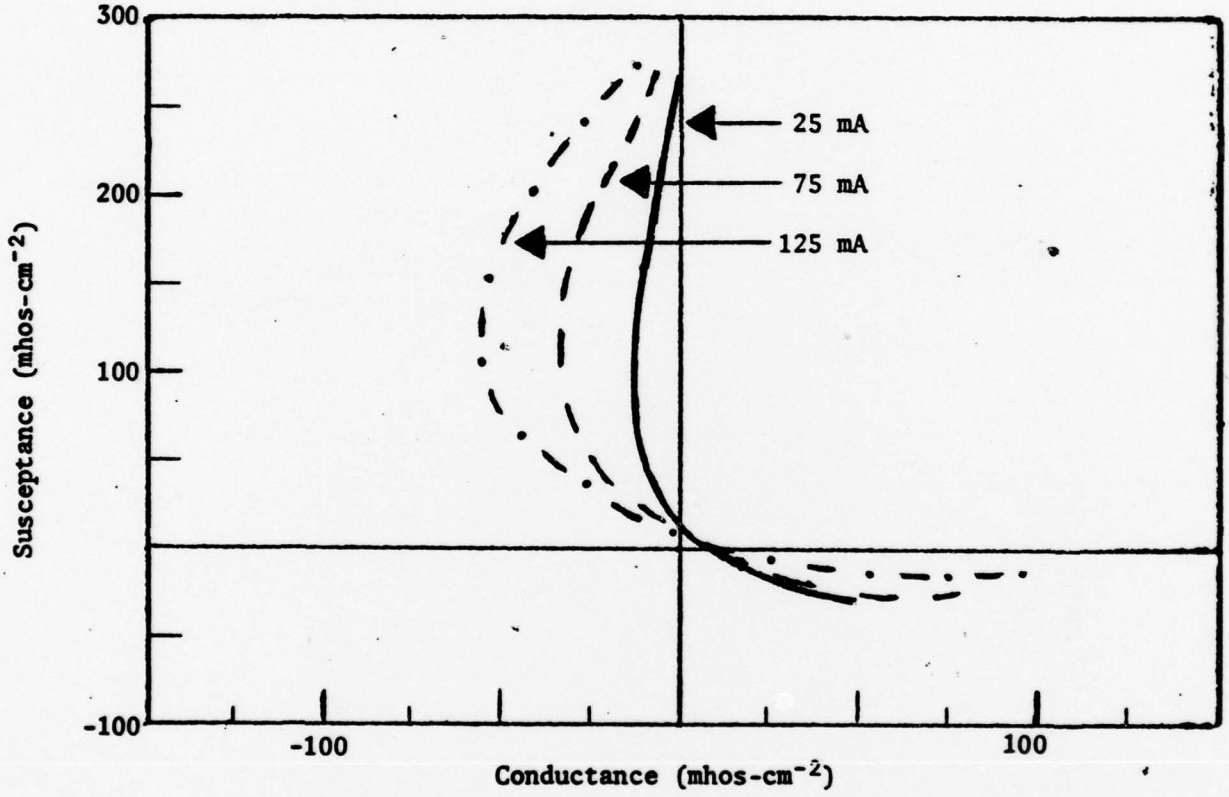

Fig. 5

Calculated Admittance for Ionization Coefficients of Salmer et al

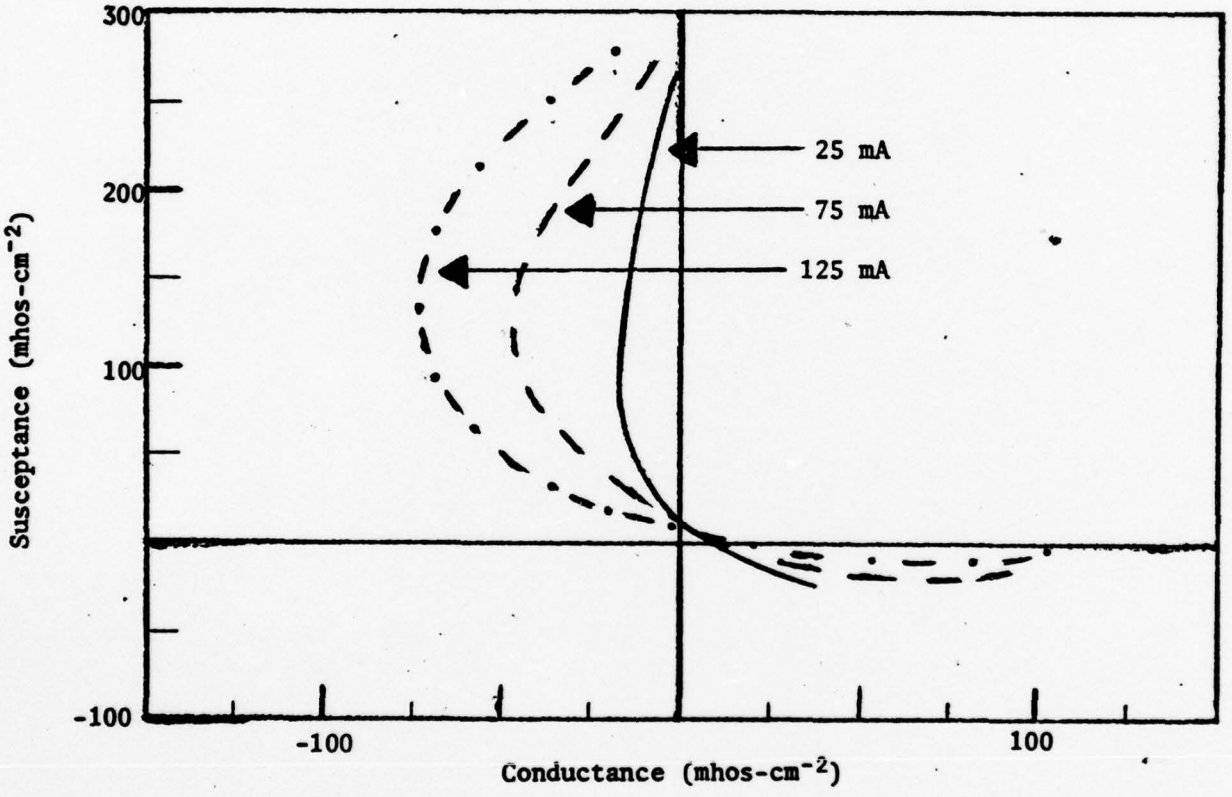

Fig. 6

Calculated Admittance for Ionization Coefficients of Wisseman et al

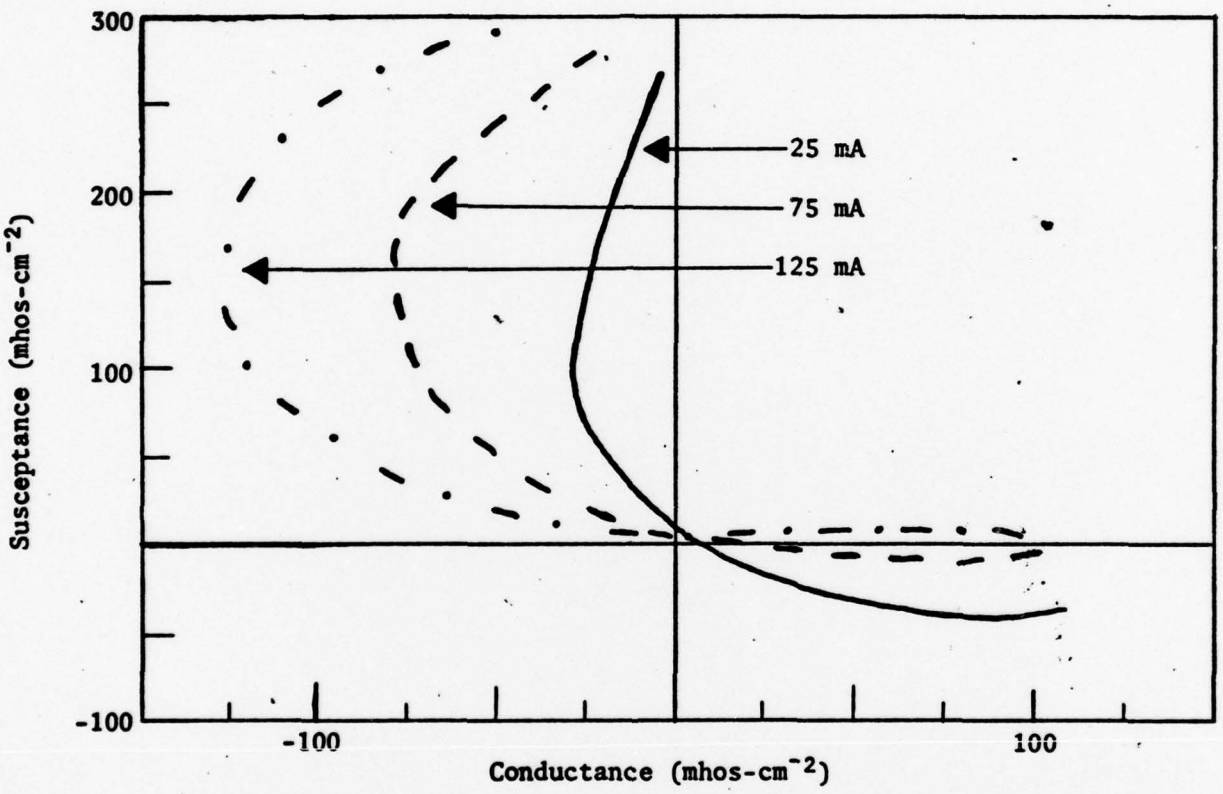

Fig. 7

Calculated Admittance for Ionization Coefficients of Ito et al

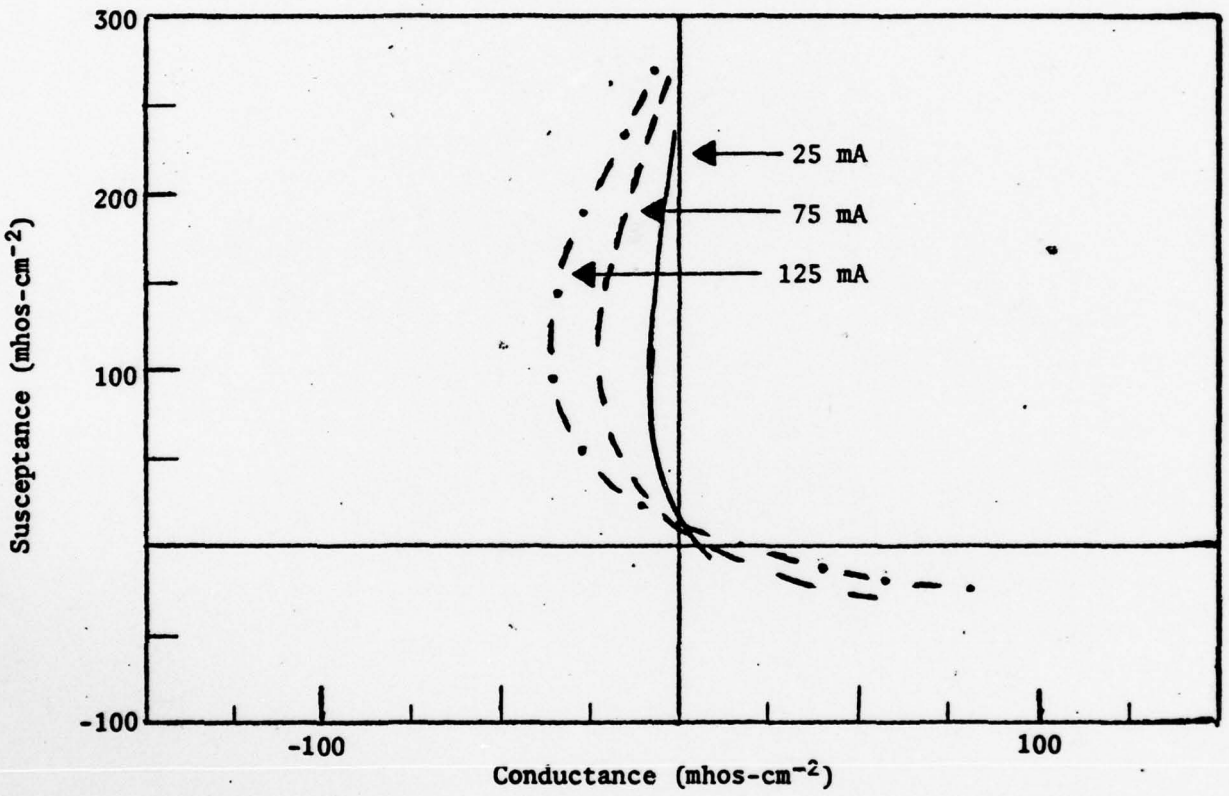

Fig. 8

Calculated Admittance for Ionization Coefficients of Okuto and Crowell

and "b" was varied between 4×10^5 and 9×10^5. Thirty-one different combinations of "a" and "b" were found to have admittance curves which are similar to the measurements, and of these the best three are shown in Figures 9, 10, and 11. The calculated outputs for the Real and Imaginary parts of the admittance for the different combinations of "a" and "b" are listed in Table II as a function of frequency and bias current.

2.4 Discussion

The exponential dependecy of the ionization rates on the electric field for the coefficients of Logan and Sze [11], Ito et al [17], and the best three computer generated values are shown in Figure 12. It is interesting to observe that a cross over exists in the high field region corresponding to $(5 - 6) \times 10^5$ V/cm. This suggests the possible existence of injection mechanisms other than avalanche multiplication in such high field regions. Indeed, a closer look at the electronic band structure of the GaAs for the <111> and <100> directions shown in Figure 13 [21], reveals the followings. In the <111> direction the energy width of the conduction band is less than the band gap, making impact ionization by electron in this band ($\Gamma_6 - L_6$) impossible. In order to initiate impact ionization, these electrons must be scattered to another conduction band. In the <100> direction, the lowest conduction band ($\Gamma_6 - X_6$) has an energy width that is larger than the band gap, but the conditions of energy conservation and momentum conservation cannot be satisfied for an electron-initiated impact-ionization event. However, these two conditions can be satisfied in the next higher band ($\Gamma_7 - X_7$). Electrons initiated impact ionization thus requires the consideration of tunneling or interconduction band scattering across the gap between these two bands. The width of this gap is about 0.2 eV [22]. In fact, the tunneling probability [23] in the range of fields corresponding to the cross-over field shown in

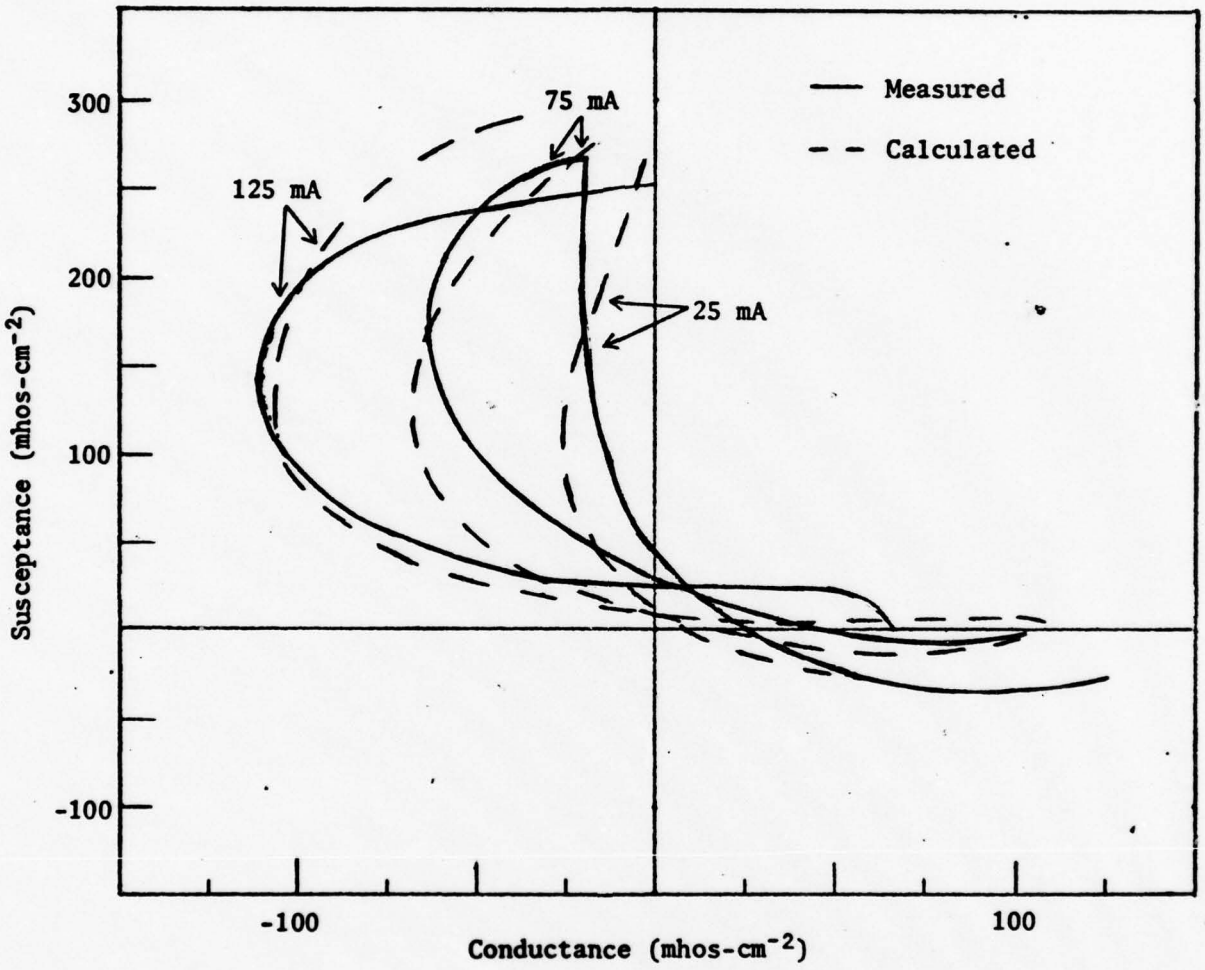

Fig. 9

Admittance for a = 4.5 × 10^5 cm^{-1} and b = 8.0 × 10^5 V/cm

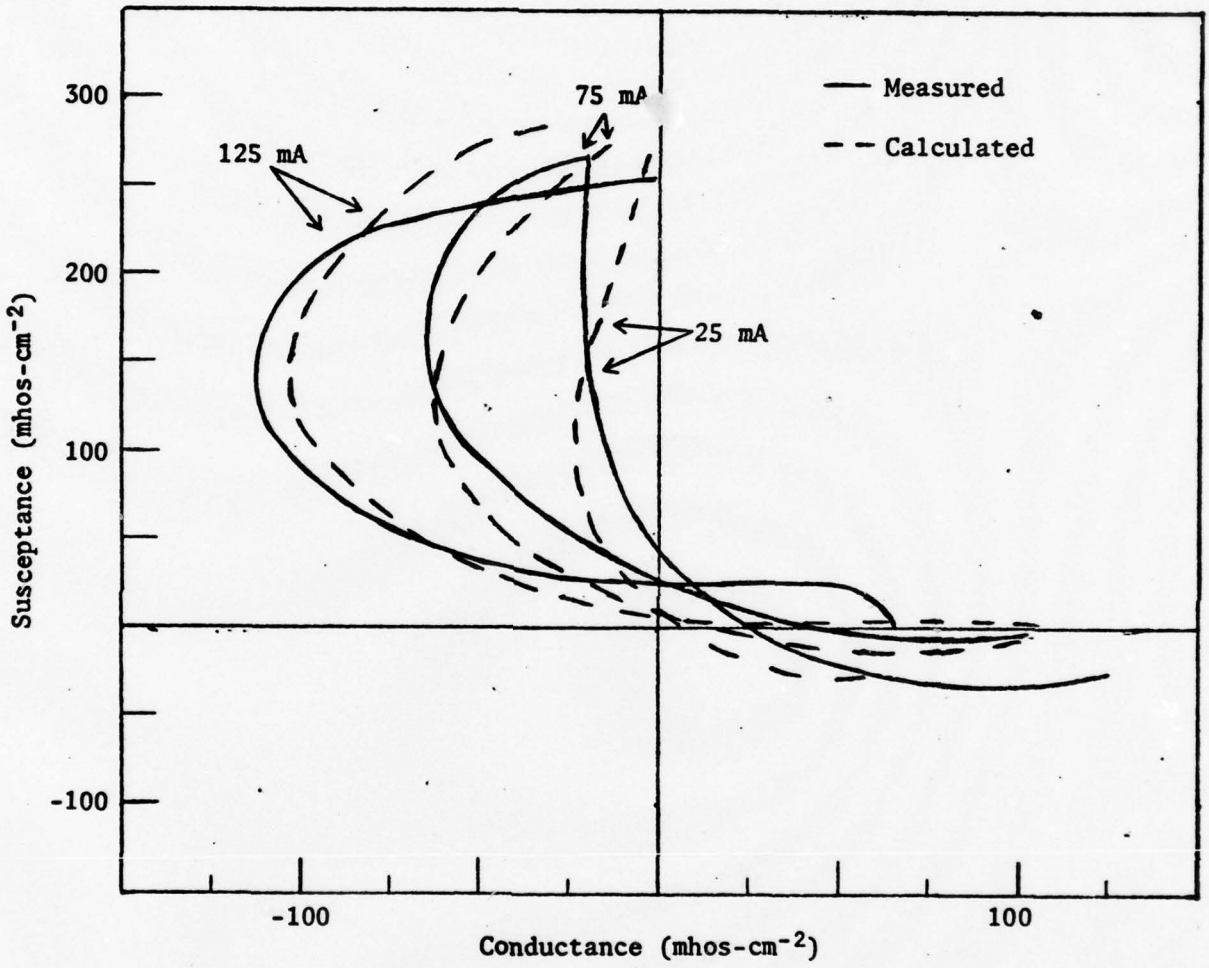

Fig. 10

Admittance for a = 6.5×10^5 cm^{-1} and b = 9.0×10^5 V/cm

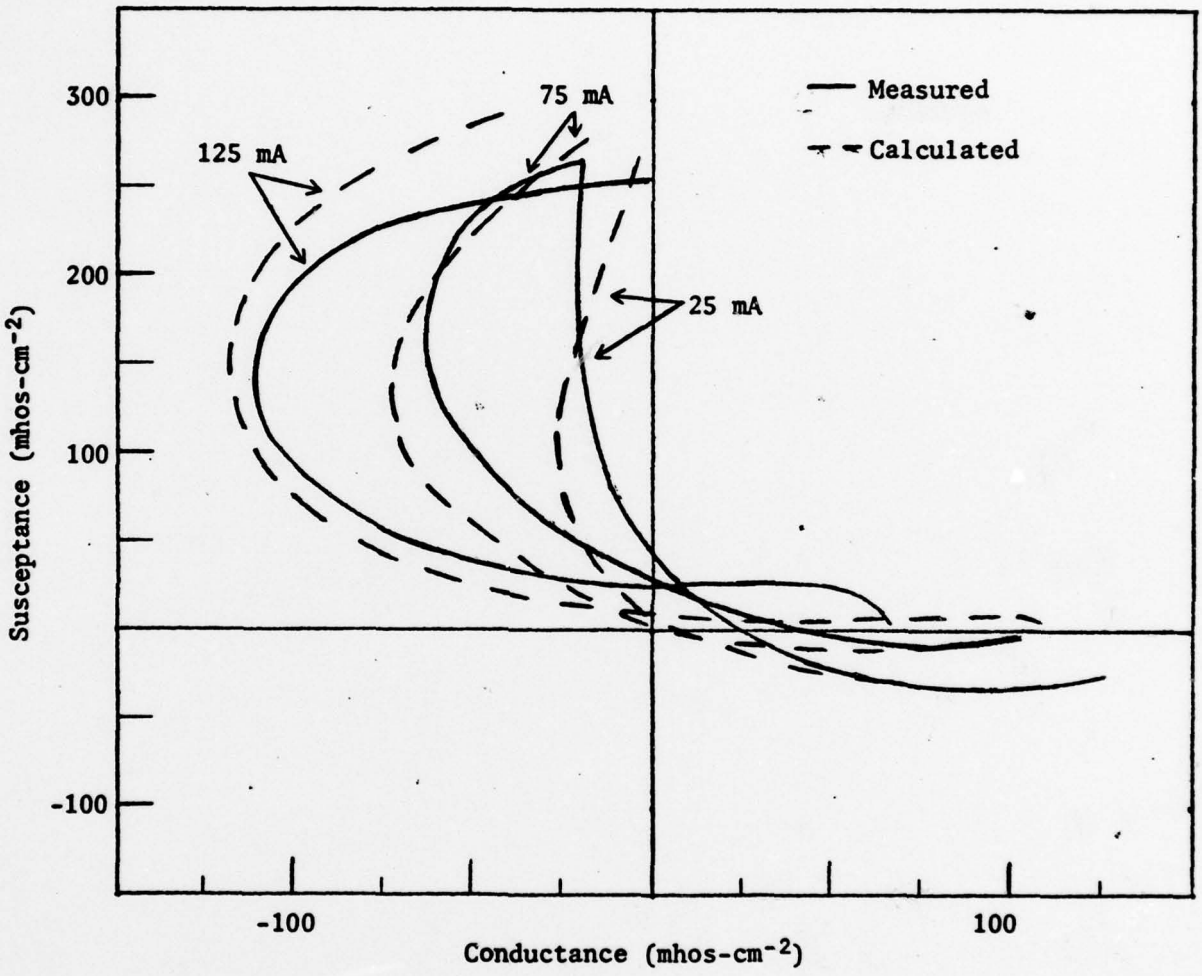

Fig. 11

Admittance for a = 7.5×10^5 cm^{-1} and b = 9.0×10^5 V/cm

Table II

Calculated admittance for different values of "a" and "b" in $\alpha = a \exp[-(b/E)^2]$

A = 0.25E 06 B = 0.50E 06

I(MIL AMP)	F(GHZ)	REAL Y(MHO*CM-2)	IMAG Y(MHO*CM-2)
25	2	0.637E 02	-0.293E 02
25	4	0.890E 01	-0.149E 01
25	6	-0.198E 02	0.546E 02
25	8	-0.263E 02	0.111E 03
25	10	-0.224E 02	0.159E 03
25	12	-0.156E 02	0.200E 03
25	14	-0.926E 01	0.236E 03
25	16	-0.451E 01	0.269E 03
75	2	0.102E 03	-0.505E 01
75	4	0.828E 02	-0.998E 01
75	6	0.420E 02	-0.839E 01
75	8	-0.203E 02	0.223E 02
75	10	-0.671E 02	0.101E 03
75	12	-0.632E 02	0.187E 03
75	14	-0.378E 02	0.243E 03
75	16	-0.172E 02	0.279E 03
125	2	0.108E 03	0.500E 01
125	4	0.100E 03	0.815E 01
125	6	0.840E 02	0.758E 01
125	8	0.487E 02	0.377E 01
125	10	-0.255E 02	0.163E 02
125	12	-0.110E 03	0.113E 03
125	14	-0.904E 02	0.238E 03
125	16	-0.389E 02	0.292E 03

A = 0.25E 06 B = 0.55E 06

I(MIL AMP)	F(GHZ)	REAL Y(MHO*CM-2)	IMAG Y(MHO*CM-2)
25	2	0.626E 02	-0.294E 02
25	4	0.801E 01	-0.536E 00
25	6	-0.198E 02	0.557E 02
25	8	-0.258E 02	0.111E 03
25	10	-0.220E 02	0.159E 03
25	12	-0.153E 02	0.200E 03
25	14	-0.905E 01	0.236E 03
25	16	-0.442E 01	0.269E 03
75	2	0.102E 03	-0.550E 01
75	4	0.818E 02	-0.106E 02
75	6	0.400E 02	-0.835E 01
75	8	-0.222E 02	0.244E 02
75	10	-0.666E 02	0.104E 03
75	12	-0.616E 02	0.188E 03
75	14	-0.367E 02	0.243E 03
75	16	-0.168E 02	0.279E 03
125	2	0.108E 03	0.469E 01
125	4	0.999E 02	0.750E 01
125	6	0.829E 02	0.664E 01
125	8	0.462E 02	0.310E 01
125	10	-0.294E 02	0.185E 02
125	12	-0.110E 03	0.118E 03
125	14	-0.871E 02	0.239E 03
125	16	-0.375E 02	0.291E 03

Table II (cont'd.)

A = 0.25E 06 B = 0.60E 06

I(MIL AMP)	F(GHZ)	REAL Y(MHO*CM-2)	IMAG Y(MHO*CM-2)
25	2	0.595E 02	-0.297E 02
25	4	0.562E 01	0.226E 01
25	6	-0.196E 02	0.587E 02
25	8	-0.245E 02	0.113E 03
25	10	-0.206E 02	0.160E 03
25	12	-0.143E 02	0.200E 03
25	14	-0.850E 01	0.236E 03
25	16	-0.415E 01	0.269E 03
75	2	0.101E 03	-0.683E 01
75	4	0.787E 02	-0.124E 02
75	6	0.341E 02	-0.784E 01
75	8	-0.271E 02	0.306E 02
75	10	-0.646E 02	0.111E 03
75	12	-0.570E 02	0.190E 03
75	14	-0.338E 02	0.243E 03
75	16	-0.155E 02	0.278E 03
125	2	0.107E 03	0.375E 01
125	4	0.987E 02	0.559E 01
125	6	0.796E 02	0.399E 01
125	8	0.387E 02	0.167E 01
125	10	-0.399E 02	0.259E 02
125	12	-0.107E 03	0.132E 03
125	14	-0.784E 02	0.242E 03
125	16	-0.339E 02	0.289E 03

A = 0.30E 06 B = 0.50E 06

I(MIL AMP)	F(GHZ)	REAL Y(MHO*CM-2)	IMAG Y(MHO*CM-2)
25	2	0.734E 02	-0.270E 02
25	4	0.188E 02	-0.982E 01
25	6	-0.189E 02	0.434E 02
25	8	-0.308E 02	0.104E 03
25	10	-0.275E 02	0.156E 03
25	12	-0.194E 02	0.200E 03
25	14	-0.114E 02	0.237E 03
25	16	-0.554E 01	0.270E 03
75	2	0.105E 03	-0.104E 01
75	4	0.909E 02	-0.351E 01
75	6	0.601E 02	-0.582E 01
75	8	0.201E 01	0.677E 01
75	10	-0.668E 02	0.711E 02
75	12	-0.810E 02	0.174E 03
75	14	-0.503E 02	0.244E 03
75	16	-0.225E 02	0.283E 03
125	2	0.109E 03	0.772E 01
125	4	0.103E 03	0.139E 02
125	6	0.921E 02	0.165E 02
125	8	0.685E 02	0.131E 02
125	10	0.139E 02	0.747E 01
125	12	-0.968E 02	0.547E 02
125	14	-0.129E 03	0.218E 03
125	16	-0.560E 02	0.299E 03

Table II (cont'd.)

A = 0.30E 06 B = 0.55E 06

I(MIL AMP)	F(GHZ)	REAL Y(MHO*CM-2)	IMAG Y(MHO*CM-2)
25	2	0.724E 02	-0.273E 02
25	4	0.176E 02	-0.901E 01
25	6	-0.192E 02	0.447E 02
25	8	-0.303E 02	0.105E 03
25	10	-0.269E 02	0.157E 03
25	12	-0.189E 02	0.200E 03
25	14	-0.112E 02	0.237E 03
25	16	-0.542E 01	0.270E 03
75	2	0.105E 03	-0.145E 01
75	4	0.902E 02	-0.422E 01
75	6	0.583E 02	-0.633E 01
75	8	-0.676E 00	0.800E 01
75	10	-0.674E 02	0.746E 02
75	12	-0.790E 02	0.175E 03
75	14	-0.488E 02	0.244E 03
75	16	-0.218E 02	0.282E 03
125	2	0.109E 03	0.745E 01
125	4	0.103E 03	0.133E 02
125	6	0.914E 02	0.155E 02
125	8	0.667E 02	0.119E 02
125	10	0.973E 01	0.743E 01
125	12	-0.100E 03	0.609E 02
125	14	-0.124E 03	0.222E 03
125	16	-0.537E 02	0.299E 03

A = 0.30E 06 B = 0.60E 06

I(MIL AMP)	F(GHZ)	REAL Y(MHO*CM-2)	IMAG Y(MHO*CM-2)
25	2	0.695E 02	-0.281E 02
25	4	0.144E 02	-0.656E 01
25	6	-0.196E 02	0.483E 02
25	8	-0.289E 02	0.107E 03
25	10	-0.253E 02	0.158E 03
25	12	-0.177E 02	0.200E 03
25	14	-0.105E 02	0.236E 03
25	16	-0.509E 01	0.269E 03
75	2	0.104E 03	-0.265E 01
75	4	0.878E 02	-0.624E 01
75	6	0.529E 02	-0.749E 01
75	8	-0.808E 01	0.122E 02
75	10	-0.684E 02	0.844E 02
75	12	-0.732E 02	0.180E 03
75	14	-0.446E 02	0.244E 03
75	16	-0.201E 02	0.281E 03
125	2	0.108E 03	0.665E 01
125	4	0.102E 03	0.116E 02
125	6	0.891E 02	0.128E 02
125	8	0.611E 02	0.872E 01
125	10	-0.247E 01	0.858E 01
125	12	-0.107E 03	0.792E 02
125	14	-0.111E 03	0.230E 03
125	16	-0.478E 02	0.296E 03

Table II (cont'd.)

A = 0.30E 06 B = 0.65E 06

I(MIL AMP)	F(GHZ)	REAL Y(MHO*CM-2)	IMAG Y(MHO*CM-2)
25	2	0.646E 02	-0.291E 02
25	4	0.970E 01	-0.232E 01
25	6	-0.198E 02	0.536E 02
25	8	-0.267E 02	0.110E 03
25	10	-0.229E 02	0.159E 03
25	12	-0.159E 02	0.200E 03
25	14	-0.944E 01	0.236E 03
25	16	-0.460E 01	0.269E 03
75	2	0.103E 03	-0.466E 01
75	4	0.836E 02	-0.940E 01
75	6	0.438E 02	-0.837E 01
75	8	-0.186E 02	0.205E 02
75	10	-0.675E 02	0.987E 02
75	12	-0.647E 02	0.186E 03
75	14	-0.388E 02	0.243E 03
75	16	-0.177E 02	0.279E 03
125	2	0.108E 03	0.527E 01
125	4	0.101E 03	0.872E 01
125	6	0.849E 02	0.841E 01
125	8	0.508E 02	0.442E 01
125	10	-0.219E 02	0.146E 02
125	12	-0.111E 03	0.108E 03
125	14	-0.934E 02	0.237E 03
125	16	-0.401E 02	0.293E 03

A = 0.30E 06 B = 0.70E 06

I(MIL AMP)	F(GHZ)	REAL Y(MHO*CM-2)	IMAG Y(MHO*CM-2)
25	2	0.578E 02	-0.298E 02
25	4	0.447E 01	0.375E 01
25	6	-0.195E 02	0.601E 02
25	8	-0.239E 02	0.114E 03
25	10	-0.200E 02	0.160E 03
25	12	-0.139E 02	0.200E 03
25	14	-0.822E 01	0.235E 03
25	16	-0.402E 01	0.269E 03
75	2	0.101E 03	-0.755E 01
75	4	0.770E 02	-0.133E 02
75	6	0.310E 02	-0.735E 01
75	8	-0.293E 02	0.340E 02
75	10	-0.634E 02	0.115E 03
75	12	-0.547E 02	0.191E 03
75	14	-0.324E 02	0.242E 03
75	16	-0.149E 02	0.277E 03
125	2	0.107E 03	0.324E 01
125	4	0.980E 02	0.457E 01
125	6	0.777E 02	0.263E 01
125	8	0.346E 02	0.124E 01
125	10	-0.448E 02	0.304E 02
125	12	-0.104E 03	0.139E 03
125	14	-0.742E 02	0.242E 03
125	16	-0.323E 02	0.289E 03

Table II (cont'd.)

A = 0.35E 06 B = 0.60E 06

I(MIL AMP)	F(GHZ)	REAL Y(MHO*CM-2)	IMAG Y(MHO*CM-2)
25	2	0.772E 02	-0.256E 02
25	4	0.239E 02	-0.128E 02
25	6	-0.178E 02	0.379E 02
25	8	-0.327E 02	0.999E 02
25	10	-0.301E 02	0.155E 03
25	12	-0.213E 02	0.200E 03
25	14	-0.125E 02	0.237E 03
25	16	-0.606E 01	0.270E 03
75	2	0.106E 03	0.544E 00
75	4	0.937E 02	-0.631E 00
75	6	0.669E 02	-0.334E 01
75	8	0.134E 02	0.297E 01
75	10	-0.623E 02	0.563E 02
75	12	-0.895E 02	0.164E 03
75	14	-0.574E 02	0.244E 03
75	16	-0.254E 02	0.284E 03
125	2	0.109E 03	0.877E 01
125	4	0.104E 03	0.161E 02
125	6	0.947E 02	0.202E 02
125	8	0.750E 02	0.182E 02
125	10	0.297E 02	0.964E 01
125	12	-0.777E 02	0.321E 02
125	14	-0.148E 03	0.199E 03
125	16	-0.668E 02	0.303E 03

A = 0.35E 06 B = 0.65E 06

I(MIL AMP)	F(GHZ)	REAL Y(MHO*CM-2)	IMAG Y(MHO*CM-2)
25	2	0.728E 02	-0.272E 02
25	4	0.181E 02	-0.935E 01
25	6	-0.191E 02	0.441E 02
25	8	-0.305E 02	0.104E 03
25	10	-0.272E 02	0.157E 03
25	12	-0.191E 02	0.200E 03
25	14	-0.113E 02	0.237E 03
25	16	-0.547E 01	0.270E 03
75	2	0.105E 03	-0.128E 01
75	4	0.905E 02	-0.392E 01
75	6	0.590E 02	-0.612E 01
75	8	0.462E 00	0.746E 01
75	10	-0.672E 02	0.731E 02
75	12	-0.798E 02	0.175E 03
75	14	-0.494E 02	0.244E 03
75	16	-0.221E 02	0.282E 03
125	2	0.109E 03	0.757E 01
125	4	0.103E 03	0.135E 02
125	6	0.917E 02	0.159E 02
125	8	0.675E 02	0.124E 02
125	10	0.115E 02	0.742E 01
125	12	-0.988E 02	0.582E 02
125	14	-0.126E 03	0.220E 03
125	16	-0.546E 02	0.299E 03

Table II (cont'd.)

A = 0.35E 06 B = 0.70E 06

I(MIL AMP)	F(GHZ)	REAL Y(MHO*CM-2)	IMAG Y(MHO*CM-2)
25	2	0.664E 02	-0.288E 02
25	4	0.113E 02	-0.388E 01
25	6	-0.198E 02	0.518E 02
25	8	-0.275E 02	0.109E 03
25	10	-0.237E 02	0.158E 03
25	12	-0.166E 02	0.200E 03
25	14	-0.979E 01	0.236E 03
25	16	-0.477E 01	0.269E 03
75	2	0.103E 03	-0.392E 01
75	4	0.852E 02	-0.828E 01
75	6	0.471E 02	-0.821E 01
75	8	-0.150E 02	0.173E 02
75	10	-0.681E 02	0.938E 02
75	12	-0.677E 02	0.184E 03
75	14	-0.407E 02	0.244E 03
75	16	-0.185E 02	0.280E 03
125	2	0.108E 03	0.578E 01
125	4	0.101E 03	0.977E 01
125	6	0.865E 02	0.999E 01
125	8	0.547E 02	0.582E 01
125	10	-0.150E 02	0.118E 02
125	12	-0.110E 03	0.977E 02
125	14	-0.994E 02	0.235E 03
125	16	-0.427E 02	0.294E 03

A = 0.35E 06 B = 0.75E 06

I(MIL AMP)	F(GHZ)	REAL Y(MHO*CM-2)	IMAG Y(MHO*CM-2)
25	2	0.579E 02	-0.298E 02
25	4	0.455E 01	0.364E 01
25	6	-0.195E 02	0.600E 02
25	8	-0.239E 02	0.114E 03
25	10	-0.200E 02	0.160E 03
25	12	-0.139E 02	0.200E 03
25	14	-0.824E 01	0.235E 03
25	16	-0.403E 01	0.269E 03
75	2	0.101E 03	-0.749E 01
75	4	0.771E 02	-0.132E 02
75	6	0.312E 02	-0.739E 01
75	8	-0.292E 02	0.337E 02
75	10	-0.635E 02	0.114E 03
75	12	-0.549E 02	0.191E 03
75	14	-0.325E 02	0.242E 03
75	16	-0.150E 02	0.277E 03
125	2	0.107E 03	0.327E 01
125	4	0.980E 02	0.465E 01
125	6	0.779E 02	0.273E 01
125	8	0.349E 02	0.126E 01
125	10	-0.445E 02	0.301E 02
125	12	-0.104E 03	0.139E 03
125	14	-0.745E 02	0.242E 03
125	16	-0.324E 02	0.289E 03

Table II (cont'd.)

A = 0.40E 06 B = 0.70E 06

I(MIL AMP)	F(GHZ)	REAL Y(MHO*CM-2)	IMAG Y(MHO*CM-2)
25	2	0.734E 02	-0.270E 02
25	4	0.188E 02	-0.984E 01
25	6	-0.189E 02	0.433E 02
25	8	-0.308E 02	0.104E 03
25	10	-0.275E 02	0.156E 03
25	12	-0.194E 02	0.200E 03
25	14	-0.114E 02	0.237E 03
25	16	-0.554E 01	0.270E 03
75	2	0.105E 03	-0.103E 01
75	4	0.909E 02	-0.349E 01
75	6	0.601E 02	-0.581E 01
75	8	0.210E 01	0.673E 01
75	10	-0.668E 02	0.709E 02
75	12	-0.811E 02	0.174E 03
75	14	-0.504E 02	0.244E 03
75	16	-0.225E 02	0.283E 03
125	2	0.109E 03	0.773E 01
125	4	0.103E 03	0.139E 02
125	6	0.921E 02	0.165E 02
125	8	0.686E 02	0.132E 02
125	10	0.140E 02	0.748E 01
125	12	-0.967E 02	0.545E 02
125	14	-0.129E 03	0.218E 03
125	16	-0.560E 02	0.299E 03

A = 0.40E 06 B = 0.75E 06

I(MIL AMP)	F(GHZ)	REAL Y(MHO*CM-2)	IMAG Y(MHO*CM-2)
25	2	0.654E 02	-0.290E 02
25	4	0.104E 02	-0.300E 01
25	6	-0.198E 02	0.528E 02
25	8	-0.270E 02	0.110E 03
25	10	-0.232E 02	0.159E 03
25	12	-0.162E 02	0.200E 03
25	14	-0.959E 01	0.236E 03
25	16	-0.467E 01	0.269E 03
75	2	0.103E 03	-0.434E 01
75	4	0.843E 02	-0.892E 01
75	6	0.452E 02	-0.633E 01
75	8	-0.171E 02	0.191E 02
75	10	-0.678E 02	0.966E 02
75	12	-0.660E 02	0.185E 03
75	14	-0.396E 02	0.243E 03
75	16	-0.180E 02	0.280E 03
125	2	0.108E 03	0.549E 01
125	4	0.101E 03	0.917E 01
125	6	0.856E 02	0.909E 01
125	8	0.525E 02	0.500E 01
125	10	-0.190E 02	0.133E 02
125	12	-0.111E 03	0.103E 03
125	14	-0.959E 02	0.237E 03
125	16	-0.412E 02	0.293E 03

Table II (cont'd.)

A = 0.40E 06 B = 0.80E 06

I(MIL AMP)	F(GHZ)	REAL Y(MHO*CM-2)	IMAG Y(MHO*CM-2)
25	2	0.552E 02	-0.298E 02
25	4	0.284E 01	0.604E 01
25	6	-0.192E 02	0.623E 02
25	8	-0.229E 02	0.115E 03
25	10	-0.190E 02	0.160E 03
25	12	-0.132E 02	0.200E 03
25	14	-0.781E 01	0.235E 03
25	16	-0.383E 01	0.268E 03
75	2	0.997E 02	-0.866E 01
75	4	0.743E 02	-0.146E 02
75	6	0.263E 02	-0.627E 01
75	8	-0.322E 02	0.392E 02
75	10	-0.613E 02	0.120E 03
75	12	-0.514E 02	0.193E 03
75	14	-0.303E 02	0.242E 03
75	16	-0.141E 02	0.277E 03
125	2	0.107E 03	0.243E 01
125	4	0.968E 02	0.297E 01
125	6	0.746E 02	0.626E 00
125	8	0.280E 02	0.107E 01
125	10	-0.516E 02	0.380E 02
125	12	-0.100E 03	0.148E 03
125	14	-0.684E 02	0.243E 03
125	16	-0.299E 02	0.287E 03

A = 0.45E 06 B = 0.75E 06

I(MIL AMP)	F(GHZ)	REAL Y(MHO*CM-2)	IMAG Y(MHO*CM-2)
25	2	0.716E 02	-0.275E 02
25	4	0.168E 02	-0.840E 01
25	6	-0.193E 02	0.456E 02
25	8	-0.299E 02	0.105E 03
25	10	-0.265E 02	0.157E 03
25	12	-0.186E 02	0.200E 03
25	14	-0.110E 02	0.237E 03
25	16	-0.533E 01	0.270E 03
75	2	0.104E 03	-0.175E 01
75	4	0.896E 02	-0.474E 01
75	6	0.569E 02	-0.666E 01
75	8	-0.261E 01	0.898E 01
75	10	-0.678E 02	0.771E 02
75	12	-0.775E 02	0.177E 03
75	14	-0.477E 02	0.244E 03
75	16	-0.214E 02	0.282E 03
125	2	0.109E 03	0.725E 01
125	4	0.103E 03	0.129E 02
125	6	0.908E 02	0.148E 02
125	8	0.653E 02	0.111E 02
125	10	0.666E 01	0.755E 01
125	12	-0.102E 03	0.655E 02
125	14	-0.121E 03	0.224E 03
125	16	-0.521E 02	0.298E 03

Table II (cont'd.)

A = 0.45E 06 B = 0.80E 06

I(MIL AMP)	F(GHZ)	REAL Y(MHO*CM-2)	IMAG Y(MHO*CM-2)
25	2	0.619E 02	-0.295E 02
25	4	0.744E 01	0.101E 00
25	6	-0.198E 02	0.564E 02
25	8	-0.255E 02	0.112E 03
25	10	-0.217E 02	0.159E 03
25	12	-0.151E 02	0.200E 03
25	14	-0.892E 01	0.236E 03
25	16	-0.435E 01	0.269E 03
75	2	0.102E 03	-0.580E 01
75	4	0.811E 02	-0.110E 02
75	6	0.387E 02	-0.828E 01
75	8	-0.234E 02	0.258E 02
75	10	-0.662E 02	0.106E 03
75	12	-0.605E 02	0.188E 03
75	14	-0.360E 02	0.243E 03
75	16	-0.165E 02	0.278E 03
125	2	0.108E 03	0.447E 01
125	4	0.997E 02	0.707E 01
125	6	0.822E 02	0.603E 01
125	8	0.445E 02	0.271E 01
125	10	-0.319E 02	0.200E 02
125	12	-0.109E 03	0.121E 03
125	14	-0.850E 02	0.240E 03
125	16	-0.367E 02	0.291E 03

A = 0.50E 06 B = 0.75E 06

I(MIL AMP)	F(GHZ)	REAL Y(MHO*CM-2)	IMAG Y(MHO*CM-2)
25	2	0.768E 02	-0.257E 02
25	4	0.234E 02	-0.126E 02
25	6	-0.179E 02	0.384E 02
25	8	-0.326E 02	0.100E 03
25	10	-0.298E 02	0.155E 03
25	12	-0.211E 02	0.200E 03
25	14	-0.124E 02	0.237E 03
25	16	-0.601E 01	0.270E 03
75	2	0.106E 03	0.406E 00
75	4	0.935E 02	-0.888E 00
75	6	0.663E 02	-0.358E 01
75	8	0.123E 02	0.323E 01
75	10	-0.628E 02	0.576E 02
75	12	-0.888E 02	0.165E 03
75	14	-0.567E 02	0.244E 03
75	16	-0.251E 02	0.284E 03
125	2	0.109E 03	0.868E 01
125	4	0.104E 03	0.159E 02
125	6	0.945E 02	0.198E 02
125	8	0.745E 02	0.177E 02
125	10	0.284E 02	0.933E 01
125	12	-0.797E 02	0.339E 02
125	14	-0.146E 03	0.201E 03
125	16	-0.658E 02	0.303E 03

Table II (cont'd.)

A = 0.50E 06 B = 0.80E 06

I(MIL AMP)	F(GHZ)	REAL Y(MHO*CM-2)	IMAG Y(MHO*CM-2)
25	2	0.677E 02	-0.285E 02
25	4	0.125E 02	-0.500E 01
25	6	-0.197E 02	0.503E 02
25	8	-0.281E 02	0.108E 03
25	10	-0.244E 02	0.158E 03
25	12	-0.170E 02	0.200E 03
25	14	-0.101E 02	0.236E 03
25	16	-0.490E 01	0.269E 03
75	2	0.103E 03	-0.339E 01
75	4	0.863E 02	-0.745E 01
75	6	0.495E 02	-0.798E 01
75	8	-0.122E 02	0.151E 02
75	10	-0.683E 02	0.900E 02
75	12	-0.699E 02	0.183E 03
75	14	-0.423E 02	0.244E 03
75	16	-0.191E 02	0.280E 03
125	2	0.108E 03	0.614E 01
125	4	0.102E 03	0.105E 02
125	6	0.876E 02	0.112E 02
125	8	0.574E 02	0.695E 01
125	10	-0.988E 01	0.102E 02
125	12	-0.110E 03	0.902E 02
125	14	-0.104E 03	0.233E 03
125	16	-0.447E 02	0.295E 03

A = 0.50E 06 B = 0.85E 06

I(MIL AMP)	F(GHZ)	REAL Y(MHO*CM-2)	IMAG Y(MHO*CM-2)
25	2	0.561E 02	-0.298E 02
25	4	0.334E 01	0.531E 01
25	6	-0.193E 02	0.616E 02
25	8	-0.232E 02	0.115E 03
25	10	-0.193E 02	0.160E 03
25	12	-0.134E 02	0.200E 03
25	14	-0.794E 01	0.235E 03
25	16	-0.389E 01	0.268E 03
75	2	0.100E 03	-0.830E 01
75	4	0.752E 02	-0.142E 02
75	6	0.278E 02	-0.666E 01
75	8	-0.314E 02	0.375E 02
75	10	-0.620E 02	0.118E 03
75	12	-0.524E 02	0.192E 03
75	14	-0.310E 02	0.242E 03
75	16	-0.143E 02	0.277E 03
125	2	0.107E 03	0.269E 01
125	4	0.972E 02	0.348E 01
125	6	0.756E 02	0.125E 01
125	8	0.301E 02	0.106E 01
125	10	-0.496E 02	0.355E 02
125	12	-0.101E 03	0.145E 03
125	14	-0.702E 02	0.243E 03
125	16	-0.306E 02	0.288E 03

Table II (cont'd.)

A = 0.55E 06 B = 0.80E 06

I(MIL AMP)	F(GHZ)	REAL Y(MHO*CM-2)	IMAG Y(MHO*CM-2)
25	2	0.727E 02	-0.272E 02
25	4	0.180E 02	-0.924E 01
25	6	-0.191E 02	0.443E 02
25	8	-0.304E 02	0.104E 03
25	10	-0.271E 02	0.157E 03
25	12	-0.190E 02	0.200E 03
25	14	-0.112E 02	0.237E 03
25	16	-0.545E 01	0.270E 03
75	2	0.105E 03	-0.133E 01
75	4	0.904E 02	-0.402E 01
75	6	0.588E 02	-0.619E 01
75	8	0.841E-01	0.764E 01
75	10	-0.673E 02	0.736E 02
75	12	-0.796E 02	0.175E 03
75	14	-0.492E 02	0.244E 03
75	16	-0.220E 02	0.282E 03
125	2	0.109E 03	0.753E 01
125	4	0.103E 03	0.135E 02
125	6	0.916E 02	0.158E 02
125	8	0.672E 02	0.123E 02
125	10	0.109E 02	0.742E 01
125	12	-0.993E 02	0.591E 02
125	14	-0.125E 03	0.221E 03
125	16	-0.543E 02	0.299E 03

A = 0.55E 06 B = 0.85E 06

I(MIL AMP)	F(GHZ)	REAL Y(MHO*CM-2)	IMAG Y(MHO*CM-2)
25	2	0.615E 02	-0.295E 02
25	4	0.709E 01	0.504E 00
25	6	-0.198E 02	0.568E 02
25	8	-0.253E 02	0.112E 03
25	10	-0.215E 02	0.159E 03
25	12	-0.149E 02	0.200E 03
25	14	-0.884E 01	0.236E 03
25	16	-0.432E 01	0.269E 03
75	2	0.102E 03	-0.600E 01
75	4	0.807E 02	-0.113E 02
75	6	0.378E 02	-0.822E 01
75	8	-0.241E 02	0.266E 02
75	10	-0.659E 02	0.107E 03
75	12	-0.598E 02	0.189E 03
75	14	-0.356E 02	0.243E 03
75	16	-0.163E 02	0.278E 03
125	2	0.108E 03	0.434E 01
125	4	0.995E 02	0.680E 01
125	6	0.817E 02	0.564E 01
125	8	0.434E 02	0.248E 01
125	10	-0.335E 02	0.211E 02
125	12	-0.109E 03	0.124E 03
125	14	-0.837E 02	0.240E 03
125	16	-0.361E 02	0.291E 03

Table II (cont'd.)

A = 0.60E 06 B = 0.80E 06

I(MIL AMP)	F(GHZ)	REAL Y(MHO*CM-2)	IMAG Y(MHO*CM-2)
25	2	0.769E 02	-0.257E 02
25	4	0.235E 02	-0.126E 02
25	6	-0.179E 02	0.383E 02
25	8	-0.326E 02	0.100E 03
25	10	-0.299E 02	0.155E 03
25	12	-0.211E 02	0.200E 03
25	14	-0.125E 02	0.237E 03
25	16	-0.602E 01	0.270E 03
75	2	0.106E 03	0.433E 00
75	4	0.935E 02	-0.837E 00
75	6	0.665E 02	-0.353E 01
75	8	0.125E 02	0.317E 01
75	10	-0.627E 02	0.574E 02
75	12	-0.889E 02	0.165E 03
75	14	-0.569E 02	0.244E 03
75	16	-0.252E 02	0.284E 03
125	2	0.109E 03	0.870E 01
125	4	0.104E 03	0.160E 02
125	6	0.945E 02	0.199E 02
125	8	0.746E 02	0.178E 02
125	10	0.286E 02	0.939E 01
125	12	-0.793E 02	0.335E 02
125	14	-0.147E 03	0.201E 03
125	16	-0.660E 02	0.303E 03

A = 0.60E Q6 B = 0.85E 06

I(MIL AMP)	F(GHZ)	REAL Y(MHO*CM-2)	IMAG Y(MHO*CM-2)
25	2	0.663E 02	-0.288E 02
25	4	0.112E 02	-0.375E 01
25	6	-0.198E 02	0.519E 02
25	8	-0.274E 02	0.109E 03
25	10	-0.236E 02	0.158E 03
25	12	-0.165E 02	0.200E 03
25	14	-0.976E 01	0.236E 03
25	16	-0.475E 01	0.269E 03
75	2	0.103E 03	-0.398E 01
75	4	0.851E 02	-0.638E 01
75	6	0.469E 02	-0.823E 01
75	8	-0.153E 02	0.176E 02
75	10	-0.681E 02	0.942E 02
75	12	-0.674E 02	0.184E 03
75	14	-0.406E 02	0.244E 03
75	16	-0.184E 02	0.280E 03
125	2	0.108E 03	0.574E 01
125	4	0.101E 03	0.968E 01
125	6	0.864E 02	0.986E 01
125	8	0.544E 02	0.569E 01
125	10	-0.156E 02	0.120E 02
125	12	-0.111E 03	0.985E 02
125	14	-0.989E 02	0.235E 03
125	16	-0.425E 02	0.294E 03

Table II (cont'd.)

A = 0.65E 06 B = 0.85E 06

I(MIL AMP)	F(GHZ)	REAL Y(MHO*CM-2)	IMAG Y(MHO*CM-2)
25	2	0.705E 02	-0.279E 02
25	4	0.155E 02	-0.744E 01
25	6	-0.195E 02	0.470E 02
25	8	-0.294E 02	0.106E 03
25	10	-0.259E 02	0.157E 03
25	12	-0.181E 02	0.200E 03
25	14	-0.107E 02	0.236E 03
25	16	-0.520E 01	0.270E 03
75	2	0.104E 03	-0.222E 01
75	4	0.887E 02	-0.553E 01
75	6	0.548E 02	-0.713E 01
75	8	-0.553E 01	0.106E 02
75	10	-0.682E 02	0.810E 02
75	12	-0.752E 02	0.179E 03
75	14	-0.460E 02	0.244E 03
75	16	-0.207E 02	0.281E 03
125	2	0.109E 03	0.694E 01
125	4	0.103E 03	0.122E 02
125	6	0.900E 02	0.138E 02
125	8	0.632E 02	0.982E 01
125	10	0.188E 01	0.796E 01
125	12	-0.105E 03	0.727E 02
125	14	-0.116E 03	0.227E 03
125	16	-0.498E 02	0.297E 03

A = 0.65E 06 B = 0.90E 06

I(MIL AMP)	F(GHZ)	REAL Y(MHO*CM-2)	IMAG Y(MHO*CM-2)
25	2	0.576E 02	-0.298E 02
25	4	0.431E 01	0.396E 01
25	6	-0.195E 02	0.603E 02
25	8	-0.238E 02	0.114E 03
25	10	-0.199E 02	0.160E 03
25	12	-0.138E 02	0.200E 03
25	14	-0.818E 01	0.235E 03
25	16	-0.400E 01	0.269E 03
75	2	0.101E 03	-0.765E 01
75	4	0.768E 02	-0.134E 02
75	6	0.306E 02	-0.726E 01
75	8	-0.296E 02	0.344E 02
75	10	-0.632E 02	0.115E 03
75	12	-0.544E 02	0.191E 03
75	14	-0.322E 02	0.242E 03
75	16	-0.148E 02	0.277E 03
125	2	0.107E 03	0.316E 01
125	4	0.979E 02	0.442E 01
125	6	0.775E 02	0.244E 01
125	8	0.340E 02	0.120E 01
125	10	-0.455E 02	0.311E 02
125	12	-0.104E 03	0.140E 03
125	14	-0.737E 02	0.243E 03
125	16	-0.320E 02	0.288E 03

Table II (cont'd.)

A = 0.70E C6 B = 0.85E 06

I(MIL AMP)	F(GHZ)	REAL Y(MHO*CM-2)	IMAG Y(MHO*CM-2)
25	2	0.743E 02	-0.267E 02
25	4	0.200E 02	-0.106E 02
25	6	-0.187E 02	0.421E 02
25	8	-0.312E 02	0.103E 03
25	10	-0.281E 02	0.156E 03
25	12	-0.198E 02	0.200E 03
25	14	-0.117E 02	0.237E 03
25	16	-0.565E 01	0.270E 03
75	2	0.105E 03	-0.663E 00
75	4	0.916E 02	-0.283E 01
75	6	0.617E 02	-0.530E 01
75	8	0.463E 01	0.569E 01
75	10	-0.660E 02	0.676E 02
75	12	-0.830E 02	0.172E 03
75	14	-0.519E 02	0.244E 03
75	16	-0.231E 02	0.283E 03
125	2	0.109E 03	0.798E 01
125	4	0.104E 03	0.144E 02
125	6	0.928E 02	0.173E 02
125	8	0.701E 02	0.143E 02
125	10	0.177E 02	0.770E 01
125	12	-0.930E 02	0.489E 02
125	14	-0.133E 03	0.215E 03
125	16	-0.583E 02	0.300E 03

A = 0.70E 06 B = 0.90E 06

I(MIL AMP)	F(GHZ)	REAL Y(MHO*CM-2)	IMAG Y(MHO*CM-2)
25	2	0.618E 02	-0.295E 02
25	4	0.732E 01	0.230E 00
25	6	-0.198E 02	0.565E 02
25	8	-0.255E 02	0.112E 03
25	10	-0.216E 02	0.159E 03
25	12	-0.150E 02	0.200E 03
25	14	-0.890E 01	0.236E 03
25	16	-0.434E 01	0.269E 03
75	2	0.102E 03	-0.587E 01
75	4	0.809E 02	-0.111E 02
75	6	0.384E 02	-0.826E 01
75	8	-0.236E 02	0.260E 02
75	10	-0.661E 02	0.106E 03
75	12	-0.603E 02	0.189E 03
75	14	-0.359E 02	0.243E 03
75	16	-0.164E 02	0.278E 03
125	2	0.108E 03	0.443E 01
125	4	0.996E 02	0.698E 01
125	6	0.820E 02	0.590E 01
125	8	0.442E 02	0.263E 01
125	10	-0.324E 02	0.204E 02
125	12	-0.109E 03	0.122E 03
125	14	-0.846E 02	0.240E 03
125	16	-0.365E 02	0.291E 03

Table II (cont'd.)

A = 0.75E 06 B = 0.85E 06

I(MIL AMP)	F(GHZ)	REAL Y(MHO*CM-2)	IMAG Y(MHO*CM-2)
25	2	0.776E 02	-0.254E 02
25	4	0.245E 02	-0.132E 02
25	6	-0.176E 02	0.373E 02
25	8	-0.330E 02	0.994E 02
25	10	-0.304E 02	0.155E 03
25	12	-0.215E 02	0.200E 03
25	14	-0.127E 02	0.237E 03
25	16	-0.612E 01	0.270E 03
75	2	0.106E 03	0.715E 00
75	4	0.940E 02	-0.312E 00
75	6	0.677E 02	-0.302E 01
75	8	0.146E 02	0.267E 01
75	10	-0.616E 02	0.547E 02
75	12	-0.905E 02	0.163E 03
75	14	-0.583E 02	0.244E 03
75	16	-0.258E 02	0.285E 03
125	2	0.109E 03	0.889E 01
125	4	0.105E 03	0.164E 02
125	6	0.949E 02	0.206E 02
125	8	0.757E 02	0.188E 02
125	10	0.314E 02	0.101E 02
125	12	-0.752E 02	0.300E 02
125	14	-0.150E 03	0.196E 03
125	16	-0.682E 02	0.303E 03

A = 0.75E 06 B = 0.90E 06

I(MIL AMP)	F(GHZ)	REAL Y(MHO*CM-2)	IMAG Y(MHO*CM-2)
25	2	0.656E 02	-0.290E 02
25	4	0.105E 02	-0.315E 01
25	6	-0.198E 02	0.527E 02
25	8	-0.271E 02	0.110E 03
25	10	-0.233E 02	0.159E 03
25	12	-0.163E 02	0.200E 03
25	14	-0.962E 01	0.236E 03
25	16	-0.469E 01	0.269E 03
75	2	0.103E 03	-0.427E 01
75	4	0.845E 02	-0.881E 01
75	6	0.456E 02	-0.831E 01
75	8	-0.167E 02	0.188E 02
75	10	-0.679E 02	0.961E 02
75	12	-0.663E 02	0.185E 03
75	14	-0.398E 02	0.243E 03
75	16	-0.181E 02	0.280E 03
125	2	0.108E 03	0.554E 01
125	4	0.101E 03	0.928E 01
125	6	0.858E 02	0.924E 01
125	8	0.529E 02	0.514E 01
125	10	-0.183E 02	0.131E 02
125	12	-0.111E 03	0.102E 03
125	14	-0.965E 02	0.236E 03
125	16	-0.415E 02	0.293E 03

Table II (cont'd.)

A = 0.80E 06 B = 0.90E 06

I(MIL AMP)	F(GHZ).	REAL Y(MHO*CM-2)	IMAG Y(MHO*CM-2)
25	2	0.690E 02	-0.282E 02
25	4	0.139E 02	-0.618E 01
25	6	-0.196E 02	0.488E 02
25	8	-0.287E 02	0.107E 03
25	10	-0.251E 02	0.158E 03
25	12	-0.175E 02	0.200E 03
25	14	-0.104E 02	0.236E 03
25	16	-0.504E 01	0.269E 03
75	2	0.104E 03	-0.283E 01
75	4	0.875E 02	-0.654E 01
75	6	0.521E 02	-0.763E 01
75	8	-0.912E 01	0.129E 02
75	10	-0.684E 02	0.858E 02
75	12	-0.724E 02	0.181E 03
75	14	-0.440E 02	0.244E 03
75	16	-0.199E 02	0.281E 03
125	2	0.108E 03	0.653E 01
125	4	0.102E 03	0.113E 02
125	6	0.888E 02	0.124E 02
125	8	0.602E 02	0.827E 01
125	10	-0.428E 01	0.892E 01
125	12	-0.108E 03	0.819E 02
125	14	-0.109E 03	0.231E 03
125	16	-0.470E 02	0.296E 03

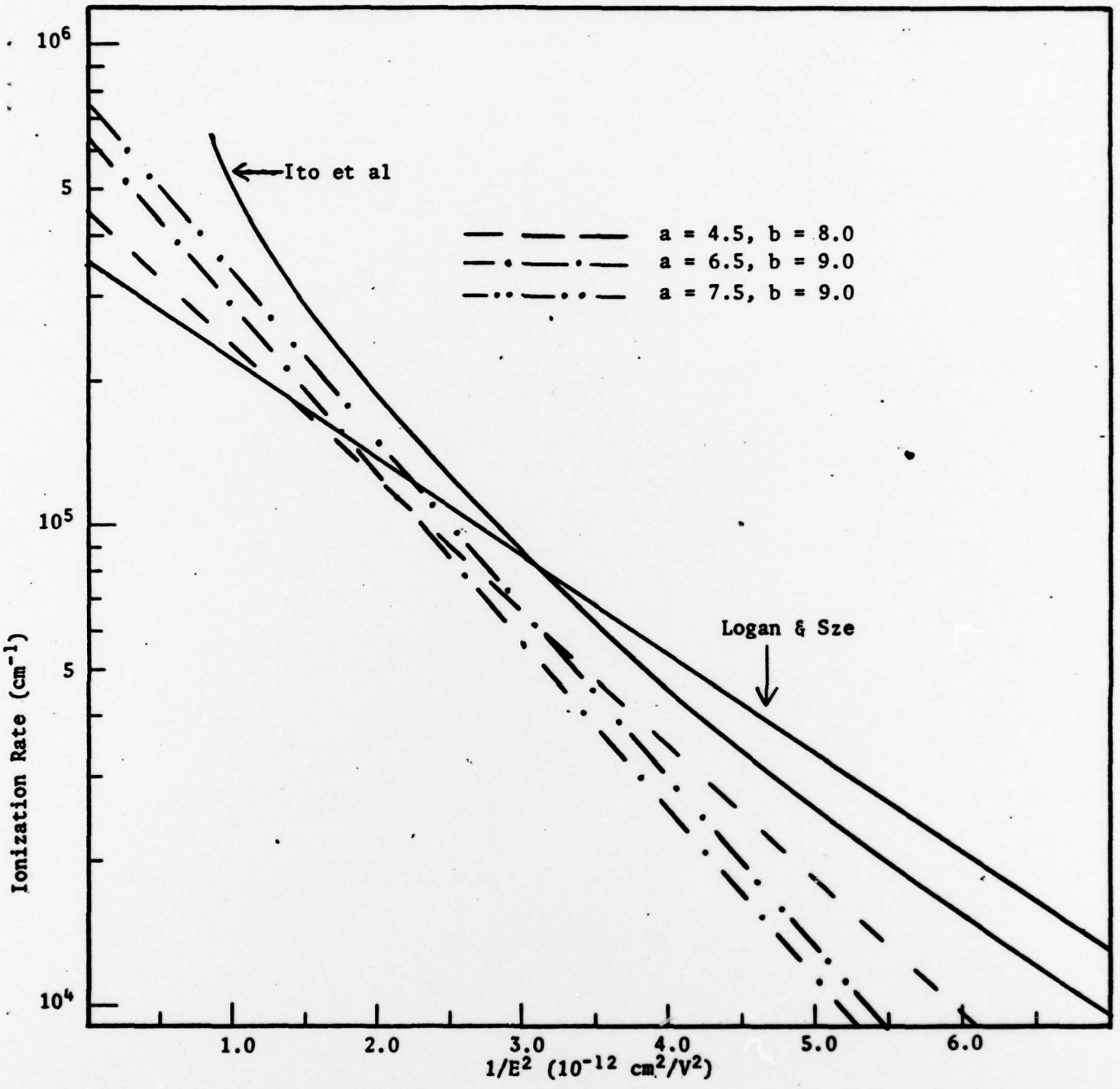

Fig. 12

Ionization Rate α as a Function of Inverse Electric Field Squared

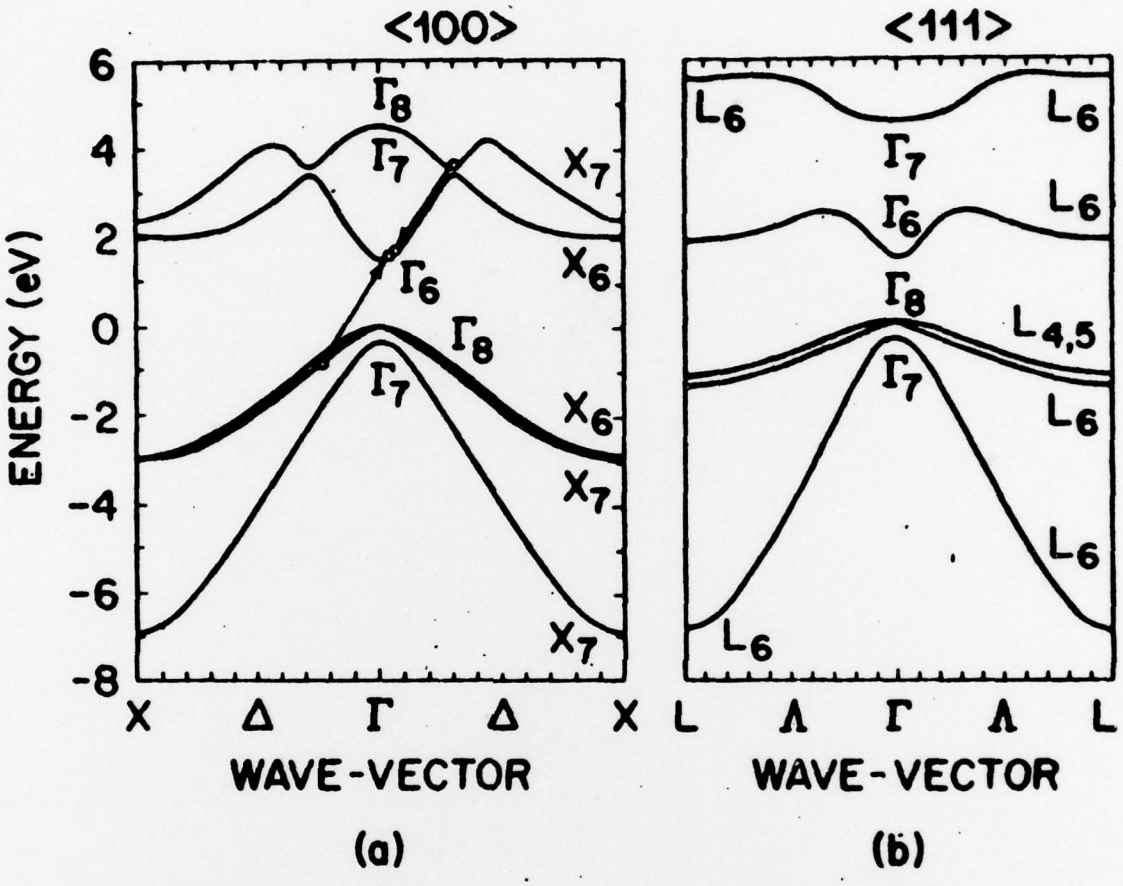

Fig. 13

Electronic Band Structure in GaAs: (a) for <100>, (b) for <111>

Figure 12 is substantial.

The tunneling time is proportional to the reciprocal of tunneling probability. Following Kane's [24] formulation, the tunneling probability per unit time, w, is:

$$w = \frac{2\pi}{\hbar} (M_{nn'})^2 \rho(E)$$

where $\rho(E)$ is the density of states given as:

$$\rho(E) = \frac{1}{\Delta E} = \frac{\kappa}{2\pi F} .$$

Here, κ = principal vector of the reciprocal lattice (length of the line k_x, k_{yo}, k_{zo} subtended by the first Brillouin zone).

F = force on the electron.

$M_{nn'}$, is the transition matrix element:

$$M_{nn'} = \frac{\pi\sqrt{M_r E_G}\, F}{3\hbar q\kappa} \exp \left\{ \frac{-\pi\hbar |q^2| E_G^{1/2}}{4FM_r^{1/2}} \right\}$$

where, M_r = reduced mass

E_G = energy-band gap, (0.2 eV)

Based on the above, the tunneling time at electric field $E = 5 \times 10^5$ V/cm and 6×10^5 V/cm are in the order of 1.2×10^{-12} sec. and 3×10^{-3} sec. respectively. On the other hand, the transit time across the high field avalanche zone whose width is 0.3 μm is estimated to be in the range $(1.11 - 3.33) \times 10^{-12}$ sec. This indicates that some electrons may pass through the high field region within shorter periods of time than what is required from the electrons to reach threshold energy and initiate ionizations. If this transit is by tunneling, resistive effects supported by such injection mechanisms are therefore induced.

SECTION III CONCLUSIONS AND RECOMENDATIONS

Investigations related to the effect of ionizaation rates on the admittance behavior of LHL GaAs Schottky IMPATT diodes have been completed successfully. Analysis and experimental results have both been supportive and indicate that at low currents the resonant frequency is less than the cuttoff frequency and that at high currents the admittance behavior is capacitive. An examination of different ionization rates has revealed that for the high field values encountered in the narrow avalanche zones other injections, such as tunneling, may coexist along with the impact ionization. Such different injections are crystal orientation dependent, are influenced by doping levels and as such should also depend on crystal perfection.

With the growing demand on GaAs for its well recognized advantages over Si and the newly emerging processing techologies in the GaAs material, such as ion-implantation and laser annealing, it is recommended that work be pursued using GaAs junction diodes fabricated by such technologies to further investigate the ionization rates. Specifically, to determine what effects the recrystallization during annealing by laser after ion-implantation would have on the ionization rates. This would be helpful for the better understanding and design of devices which operates on the principle of avalanche multiplication such as avalanche photodiodes, FAMOS (Floating gate Avalanche injection MOS transistors), in addition to IMPATT diodes. Furthermore, it should also provide useful information in the development of monolithic GaAs microwave IC transmitters and receivers.

REFERENCES

[1] S.M. Sze, Physics of Semiconductor Devices, New York:Wiley, 1969.

[2] J. Ruch and W. Fawcett, "Temperature Dependence of the Transport Properties of GaAs Determined by a Monte-Carlo Method," J. Appl. Phys. Vol. 41, p. 3843, August 1970.

[3] C.A. Lechti, "Microwave Field Effect Transistors-1976," IEEE Trans. Microwave Theory & Techniques, MTT-24, p. 279, June 1976.

[4] R.C. Eden, "The Prospects for Ultra-High Speed VLSI GaAs Digital Logic," IEEE Trans. Electron Devices, ED-25, p. 1339, Nov. 1978.

[5] K.G. McKay and K.B. McAjee, "Electron Multiplication in Silicon and Germanium" Phys. Rev., Vol. 91, p. 1079, 1953.

[6] S.L. Miller, "Ionization Rates for Holes and Electrons in Silicon," Phys. Rev., Vol. 105, p. 1246, 1957.

[7] P.A. Wolf, "Theory of Electron Multiplication in Silicon and Germanium," Phys. Rev., Vol. 95, p. 1415, 1954.

[8] G.A. Baraff, "Distribution Functions and Ionization Rates for Hot Electrons in Semiconductors," Phys. Rev., Vol. 128, p. 2507, 1962.

[9] D.L. Schurfetter and H.K. Gummel, "Large-Signal Analysis of a Silicon Read Diode Oscillator," IEEE Trans. Electron Devices, Vol. ED-16, pp. 64-77, Jan. 1969.

[10] C.T. Rucker, J.W. Amoss, G.N. Hill, N.W. Cox, H.M. Harris, and D.W. Covington, "IMPATT Diodes Chip Level Combining," Interim Report (Georgia Tech), Nov. 1976, Contract No. F33615-74-C-1020.

[11] R.A. Logan and S.M. Sze, "Avalanche Multiplication in Ge and GaAs p-n Junction," J. Phys. Jap. Syppl., Vol. 21, p. 434, 1966.

[12] R. Hall and J.H. Leck, "Avalanche Breakdown of Gallium Arsenide p-n Junctions," International J. of Electronics, p. 259, Dec. 1968.

[13] S.M. Sze and G. Gibbons, "Avalanche Breakdown Voltages of Abrupt and Linearly Graded p-n Junctions in Ge, GaAs, and GaP," Appl. Phys. Lett., Vol. 8, p. 111, March 1966.

[14] G. Salmer, J. Pribetich, A. Farrayre, and B. Kramer, "Theoretical and Experimental Study of GaAs IMPATT Oscillator Efficiency," J. of Appl. Phys., Vol. 44, p. 314, Jan 1973.

[15] W.R. Wissenman, D.W. Shaw, R.L. Adams, and T.E. Hasty, "GaAs Schottky-Read Diodes for X-Band Operation," IEEE Trans. on Electron Devices, ED-21, p. 317, June 1974.

[16] G.E. Srillman, C.M. Wolfe, A.J. Rossi and A.G. Foyt, "Unequal Electron and Hole Impact Ionization Coefficients in GaAs," Appl. Phys. Lett., Vol. 24, p. 470, May 1974.

[17] M. Ito, S. Kagawa, T. Kaneda and T. Yamaoka, "Ionization Rates for Electrons and Holes in GaAs," J. of Appl. Phys., Vol. 49, p. 4607, Aug. 1978.

[18] Y. Okuto and C.R. Crowell, "Threshold Energy Effect on Avalanche Breakdown Voltage in Semiconductor Junctions," Solid State Electronics, Vol. 18, p. 161, 1975.

[19] C.A. Lee, R.A. Logan, R.L. Batdorf, J.J. Kleimack and W. Wiegmann, "Ionization Rates of Holes and Electrons in Silicon," Phys. Rev., Vol. 134, p. 2761, 1964.

[20] M. Gliden and M.E. Hines, "Electronic Tuning Effects in the Read Microwave Avalanche Diode," IEEE Trans. Electron Devices, ED-13, p. 169, Jan. 1969.

[21] T.P. Pearsall and R.E. Nahory, "Orientation Dependence of Free-Carrier Impact Ionization in Semiconductors: GaAs," Phys. Rev. Lett., Vol. 39, p. 295, August, 1977.

[22] R. Chilkowsky and M.L. Cohen, "Nonlocal Psudopotential Calculations for the Electronic Sturcture of Eleven Diamond and Zinc-Blende Semiconductors," Phys. Rev., B-14, p. 556, 1976.

[23] E.O. Kane, "Zener Tunneling in Semiconductors," J. Phys. Chem. Solids, 12, p. 131, 1959.

[24] E.O. Kane, "Zener Tunneling in Semiconductors," J. Phys. Solids, Vol. 12, p. 181, 1959.